The Plant Cell, Vol. 21: 1195–1211, April 2009, www.plantcell.org

The RNA Binding Protein ELF9 Directly Reduces *SUPPRESSOR OF OVEREXPRESSION OF CO1* Transcript Levels in *Arabidopsis*, Possibly via Nonsense-Mediated mRNA Decay[W]

Hae-Ryong Song,[a,b] Ju-Dong Song,[a] Jung-Nam Cho,[a,b] Richard M. Amasino,[b,c] Bosl Noh,[b,d,1] and Yoo-Sun Noh[a,b,1]

[a] School of Biological Sciences, Seoul National University, Seoul 151-747, Korea
[b] Global Research Laboratory for Floral Regulatory Signaling, Seoul National University, Seoul 151-747, Korea
[c] Department of Biochemistry, University of Wisconsin, Madison, Wisconsin 53706
[d] Environmental Biotechnology National Core Research Center, Gyeongsang National University, Jinju 660-701, Korea

***SUPPRESSOR OF OVEREXPRESSION OF CO1* (*SOC1*) is regulated by a complex transcriptional regulatory network that allows for the integration of multiple floral regulatory inputs from photoperiods, gibberellin, and *FLOWERING LOCUS C*. However, the posttranscriptional regulation of *SOC1* has not been explored. Here, we report that EARLY FLOWERING9 (ELF9), an *Arabidopsis thaliana* RNA binding protein, directly targets the *SOC1* transcript and reduces *SOC1* mRNA levels, possibly through a nonsense-mediated mRNA decay (NMD) mechanism, which leads to the degradation of abnormal transcripts with premature translation termination codons (PTCs). The fully spliced *SOC1* transcript is upregulated in *elf9* mutants as well as in mutants of NMD core components. Furthermore, a partially spliced *SOC1* transcript containing a PTC is upregulated more significantly than the fully spliced transcript in *elf9* in an ecotype-dependent manner. A Myc-tagged ELF9 protein (MycELF9) directly binds to the partially spliced *SOC1* transcript. Previously known NMD target transcripts of *Arabidopsis* are also upregulated in *elf9* and recognized directly by MycELF9. *SOC1* transcript levels are also increased by the inhibition of translational activity of the ribosome. Thus, the *SOC1* transcript is one of the direct targets of ELF9, which appears to be involved in NMD-dependent mRNA quality control in *Arabidopsis*.**

INTRODUCTION

The timing of the transition to flowering is critical for the success of the next generation, and each plant species has evolved finely tuned mechanisms to properly respond to environmental cues as well as to internal developmental signals. Molecular genetic studies of the model plant *Arabidopsis thaliana* have revealed several major pathways that are involved in the regulation of flowering time. The photoperiod pathway mediates the daylength signal, which is perceived mainly in the leaves by photoreceptors, such as phytochromes and cryptochromes. Upon perception of inductive photoperiods, a graft-transmissible signal, which is likely to be FLOWERING LOCUS T (FT) protein, is translocated from the leaves to the shoot apex, where it partners with FD to stimulate the floral transition (Abe et al., 2005; Wigge et al., 2005; reviewed in Zeevaart, 2008). *CONSTANS* (*CO*; Putterill et al., 1995) acts as an *FT* activator in the photoperiod pathway. In *Arabidopsis*, the transcriptional activity of *CO* is regulated by the circadian clock through *GIGANTEA* (*GI*) and *CYCLING DOF FACTOR1* (Imaizumi et al., 2005; Mizoguchi et al., 2005). *CO* activity is also regulated at the protein level by a ubiquitin (UBQ)-dependent proteolysis pathway that involves the function of *CONSTITUTIVE PHOTOMORPHOGENIC1* (Liu et al., 2008b; Jang et al., 2008) and *SUPPRESSOR OF PHYA-105* (Laubinger et al., 2006).

Another major environmental cue for plants in temperate climates can be exposure to winter cold. The promotion of flowering by such exposure is known as vernalization (reviewed in Sung and Amasino, 2005). In *Arabidopsis*, this promotion results from the epigenetic silencing of the flowering repressor *FLOWERING LOCUS C* (*FLC*; Michaels and Amasino, 1999; Sheldon et al., 1999). The winter-annual habit in *Arabidopsis* is conferred by dominant functional alleles of *FRIGIDA* (*FRI*) and *FLC* (Koornneef et al., 1994; Lee et al., 1994). *FRI* acts as an activator of *FLC*, and the role of vernalization is to antagonize the activity of *FRI* on *FLC* expression. Certain late-flowering mutants exhibit winter-annual flowering time behavior similar to that of *FRI*-containing accessions (Koornneef et al., 1991); the genes defined by these mutants are called autonomous pathway genes (Koornneef et al., 1991). The autonomous pathway genes, which act as *FLC* repressors, encode proteins of primarily of two types: (1) putative RNA binding proteins, such as *FCA* (Macknight et al., 1997), *FPA* (Schomburg et al., 2001), *FY* (Simpson et al., 2003), and *FLOWERING LOCUS K* (Lim et al., 2004); and (2) chromatin modifiers (He and Amasino, 2005; Noh and Noh, 2006), such as *FLOWERING LOCUS D* (*FLD*; He et al., 2003), *FVE* (Ausin et al., 2004), *RELATIVE OF EARLY FLOWERING6* (Noh et al., 2004), and *HISTONE*

[1] Address correspondence to bnoh2003@yahoo.co.kr or ysnoh@snu.ac.kr.
The authors responsible for distribution of materials integral to the findings presented in this article in accordance with the policy described in the Instructions for Authors (www.plantcell.org) are: Bosl Noh (bnoh2003@yahoo.co.kr) and Yoo-Sun Noh (ysnoh@snu.ac.kr).
[W]Online version contains Web-only data.
www.plantcell.org/cgi/doi/10.1105/tpc.108.064774

ACETYLTRANSFERASEs OF THE CBP FAMILY (Han et al., 2007). In summary, *FLC*, the major floral repressor in *Arabidopsis*, acts as a convergence point of multiple floral regulatory inputs that include *FRI*, vernalization, and the autonomous pathway.

FLC is part of a gene family with five other genes encoding MADS box proteins (*MADS AFFECTING FLOWERING1* [*MAF1*] to *MAF5*; Parenicova et al., 2003) in *Arabidopsis*. Previous studies showed that some of these *MAF* genes are coregulated with *FLC* (He et al., 2004; Deal et al., 2005; Kim et al., 2005; Han et al., 2007). One of them, *MAF1* (which is also called *FLOWERING LOCUS M* [*FLM*]), is known to repress flowering primarily under noninductive photoperiods (Scortecci et al., 2001). Another gene, *MAF2*, prevents premature vernalization in response to brief cold spells (Ratcliffe et al., 2003).

The floral promotion and repressing pathways converge at a few floral integrators, such as *FT*, *SUPPRESSOR OF OVEREXPRESSION OF CO1* (*SOC1*), and *LEAFY* (*LFY*) (reviewed in Simpson and Dean, 2002). The photoperiodic floral promotion activity mediated by CO is counteracted by the floral repressive activity of FLC, and these antagonizing signals activate and repress *FT* and *SOC1* expression, respectively. *SOC1* is also involved in integrating gibberellin (GA)-dependent floral promotion signals (Moon et al., 2003), and *LFY* integrates photoperiodic and GA signals through discrete *cis*-elements in the promoter (Blázquez and Weigel, 2000).

SOC1 is regulated by CO and FLC via separate promoter elements (Hepworth et al., 2002). Although it is not known whether CO regulates *SOC1* directly, the effect of FLC on *SOC1* is direct (Hepworth et al., 2002; Searle et al., 2006). The molecular mechanisms underlying the positive effect of GA on *SOC1* transcription remain elusive. Recently, AGAMOUS-LIKE24 (AGL24), another MADS box protein, and SOC1 were shown to form a positive feedback loop that enhances the transcription of both *AGL24* and *SOC1* during the floral transition (Liu et al., 2008a). The FT-FD complex in the shoot apex also has a positive effect on *SOC1* transcription during floral transition, possibly through an indirect mechanism (Wigge et al., 2005). SHORT VEGETATIVE PHASE (SVP), a MADS box protein that can interact with FLC in vegetative tissues, has been reported to directly repress *SOC1* transcription in the shoot apex (Li et al., 2008).

Therefore, *SOC1* is subject to a regulatory network that allows for the integration of multiple floral regulatory inputs. However, posttranscriptional regulation of *SOC1* has not been reported. In this study, we demonstrate that EARLY FLOWERING9 (ELF9), an *Arabidopsis* RNA binding protein, directly targets *SOC1* transcripts and regulates their expression, possibly through a nonsense-mediated mRNA decay (NMD) mechanism (reviewed in Isken and Maquat, 2008), which detects premature translation termination codons (PTCs) and allows for the degradation of PTC-containing abnormal transcripts.

RESULTS

Loss of *ELF9* Function in the Wassilewskija Ecotype Causes Early Flowering in Short Days

The *early flowering9-1* (*elf9-1*) mutant was isolated from an *Arabidopsis* T-DNA insertion mutant population generated in the Wassilewskija (Ws) accession based on its early flowering phenotype in noninductive short days (SDs; 8 h of light and 16 h of dark). The *elf9-1* mutant flowered with 11 to ~12 rosette leaves, while wild-type Ws plants flowered with 32 to ~33 rosette leaves in SD (Figures 1A and 1B). The early flowering phenotype was not obvious in inductive long days (LDs; 16 h of light and 8 h of dark), as both the mutant and wild type flowered with approximately six to seven rosette leaves (Figure 1B). The *elf9-1* mutant also exhibited a smaller leaf size than the wild type in SDs (Figure 1A). However, this might be due to the early flowering of *elf9-1* in SDs because there was no significant difference in body size between the mutant and the wild type in LDs, under which the flowering times were not significantly different. A segregation analysis based on flowering time revealed that the *elf9-1* mutation is recessive (13 out of 50 progenies of an *elf9-1* heterozygous plant flowered with 11.7 ± 0.9 rosette leaves, while the remaining 37 progenies flowered with 31.4 ± 1.7 rosette leaves in SDs).

Because *elf9-1* was isolated from a T-DNA insertion population, thermal asymmetrical interlaced PCR (see Methods) was employed to obtain the sequence of T-DNA flanking insertion sites and resulted in the identification of a T-DNA in the 14th exon of *At5g16260* (Figure 1C). This T-DNA demonstrated cosegregation with the early flowering phenotype in a large segregating population (22 out of 96 progenies of an *elf9-1* heterozygous plant flowered early in SDs, and all of the early flowering progenies were homozygous for the T-DNA insertion). To test whether the early flowering in *elf9-1* is caused by the T-DNA insertion in *At5g16260*, the *elf9-1* mutant plants were transformed with a 5.5-kb genomic DNA fragment containing the 693-bp upstream region, the entire coding region, and the 1.3-kb 3′ untranslated region (UTR) of *At5g16260*. The early flowering phenotype of *elf9-1* was fully rescued in three independent transgenic lines containing this genomic fragment (Figures 1D and 1E), demonstrating that *At5g16260* is *ELF9*.

ELF9 encodes a protein with two RNA recognition motifs (RRMs), each encoded by three exons (Figure 1C). The *Arabidopsis* genome has 196 RRM-containing protein-encoding genes (Lorkovic and Barta, 2002). The two RRMs of ELF9 showed little sequence homology to any other *Arabidopsis* RRMs. Rather, these motifs were most similar to the RRMs of yeast CUS2 and human Tat stimulatory factor 1 (Tat-SF1; Figure 1F). CUS2 is reported to be a splicing factor that aids the assembly of the splicing-competent U2 small nuclear ribonucleoprotein (Yan et al., 1998). Tat-SF1 is essential for HIV replication because recruitment of Tat-SF1 to the HIV promoter provides elongation factors important for Tat-enhanced HIV-1 transcription (Zhou and Sharp, 1996).

Spatial Expression Pattern and Nuclear Localization of ELF9

To study the spatial expression pattern of *ELF9*, genomic DNA containing the 0.6-kb promoter along with the entire coding region of *ELF9* was cloned in frame with the *β-glucuronidase* (*GUS*) reporter gene (see Methods). The GUS expression pattern was studied by histochemical GUS staining in at least 12 independent transgenic lines. Although the expression levels varied slightly, a common spatial expression pattern was observed among different transgenic lines. GUS expression was most

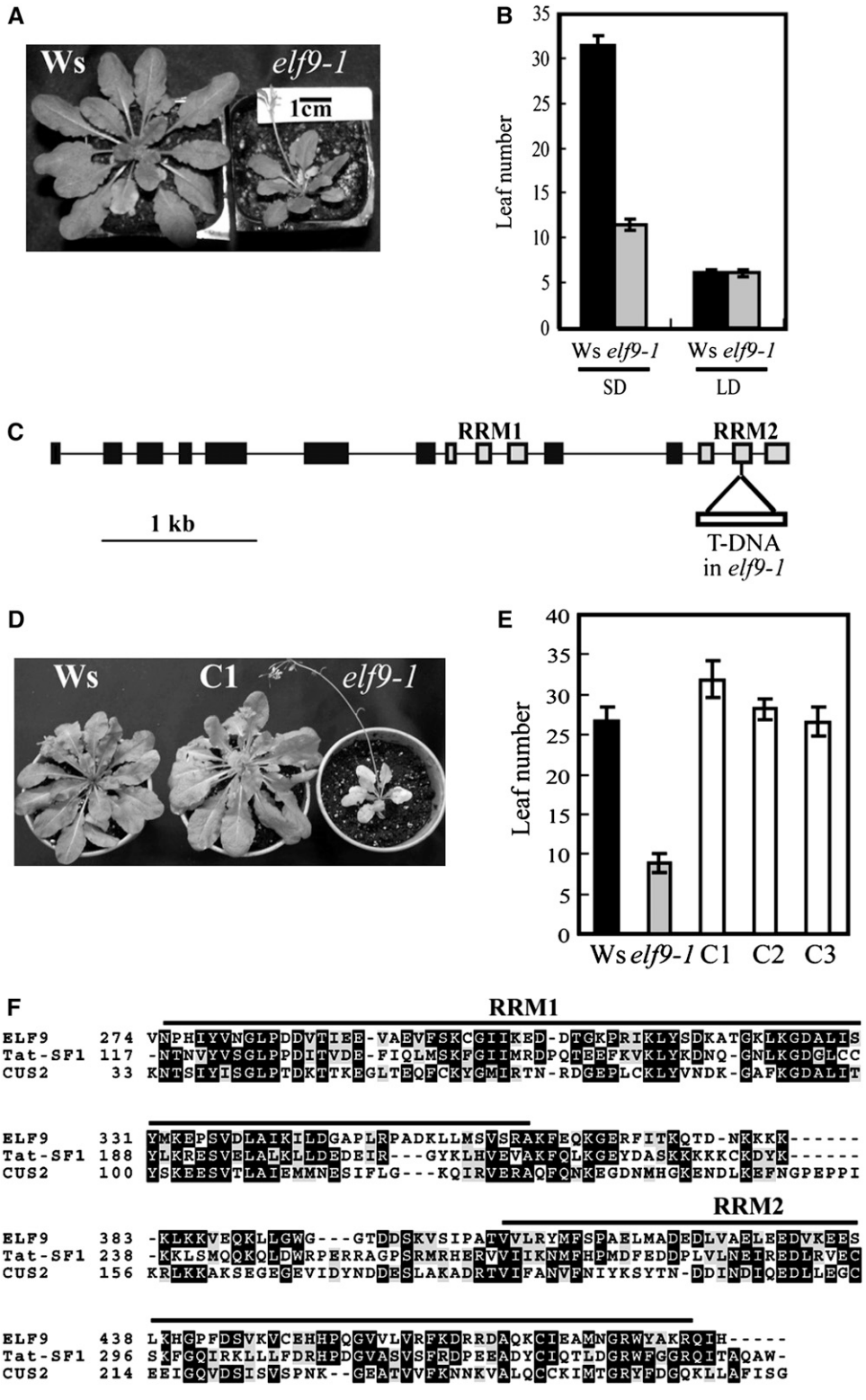

Figure 1. Early Flowering of *elf9-1* in SDs and Identification of the *ELF9* Gene.

(A) Wild-type Ws and the *elf9-1* mutant grown for 63 days (d) in SD.

(B) Flowering time of Ws (black boxes) and *elf9-1* (gray boxes) plants. Wild-type Ws and *elf9-1* mutants were grown under SD and LD conditions, and

notable in the vascular tissues of cotyledons and in the shoot apices as well as in the root tips of 10-d-old seedlings (see Supplemental Figures 1A and 1B online). GUS expression was observed in the stigma, anthers, and filaments of flowers (see Supplemental Figure 1C online).

The presence of the two RRMs in ELF9 suggested that ELF9 might be either a nuclear or cytoplasmic protein, since RNA binding proteins may have roles both in nucleus or cytoplasm. Thus, to verify the subcellular localization of ELF9, we introduced an *ELF9:GFP* fusion construct containing the cauliflower mosaic virus *35S* (*CaMV35*) promoter and the entire coding region of *ELF9*, followed by the in-frame green fluorescent protein (GFP) into wild-type Ws plants. As shown in Supplemental Figures 1D to 1K online, GFP fluorescence was detected within the nuclei of the seedling hypocotyl cells of two independent transgenic plants. However, cytoplasmic GFP fluorescence was hardly detected in any of the cells examined. Thus, the ELF9:GFP fusion protein is specifically or preferentially localized within nuclei in *Arabidopsis*.

The Levels of Fully Spliced and Incompletely Spliced Forms of *SOC1* Transcript Are Increased in *elf9-1*

To understand the underlying molecular events that induce early flowering of *elf9-1*, we compared the expression levels of various flowering genes in wild-type Ws with those present in *elf9-1* mutants by RT-PCR analysis at PCR cycles within the range of increasing productivity (Figure 2; see Supplemental Figure 2 online). In this study, the expression levels of genes acting in the photoperiod pathway, such as *CRY2*, *GI*, *CO*, and *FT*, were not altered by the *elf9-1* mutation at two different zeitgeber (ZT; number of hours after light-on) time points in SDs (Figure 2A), and the expression of *FLC*, several *FLC* family MADS genes (*FLM*, *MAF2* to *MAF5*, and *SVP*), and several *FLC* repressors (*FCA*, *FY*, *FVE*, and *FLD*) was unaffected (Figure 2A). However, the transcript level of *SOC1*, as studied using the SOC1F and SOC1R primers (see RT-PCR in Methods), was higher in *elf9-1* mutants than in the wild type at both ZT4 and ZT16 (Figure 2A).

The *SOC1* transcript level was reported to show diurnal rhythms during the day, peaking at ZT2 to ZT3 (El-Din El-Assal et al., 2003). Therefore, the diurnal expression pattern of the *SOC1* transcript was examined in both wild-type Ws and *elf9-1* mutant plants to evaluate whether the increased level of *SOC1* transcript is due to a phase shift caused by the *elf9-1* mutation. The *SOC1* transcript demonstrated oscillation and peaked at ZT4 in both wild-type and *elf9-1* mutant plants grown in SDs, as determined by RT-PCR analysis at two different nonsaturating PCR cycles (Figure 2B). However, the level of *SOC1* transcript was higher in *elf9-1* than in wild-type plants at all time points examined, indicating that the change in abundance of *SOC1* transcript is not due to a phase shift in the *SOC1* diurnal expression pattern. Rather, these data show that ELF9 is involved in the repression of *SOC1* expression.

In addition to the increased level of *SOC1* transcript in *elf9-1* mutants throughout the diurnal cycle, we also observed an increased level of a higher molecular weight DNA band in the mutants in all *SOC1* RT-PCR samples analyzed (Figures 2A and 2B). The band was ~520 bp in size (Figure 2B). The primers used in these RT-PCR analyses (SOC1F and SOC1R; see Figure 4A and Methods) should amplify a 401-bp band for fully spliced *SOC1* mRNA and an ~1.1-kb band for PCR products amplifying genomic *SOC1*. Thus, the band obtained was not amplified from genomic *SOC1* but was thought to be a product of the *SOC1* transcript. This higher molecular weight putative product of *SOC1* transcript showed the same diurnal expression pattern exhibited by fully spliced *SOC1* mRNA, and its levels were increased in the *elf9-1* mutants at all ZTs examined compared with wild-type plants. For more careful validation of the higher molecular weight band, we PCR amplified *SOC1* cDNA using primers designed to detect full-length *SOC1* cDNA (SOC1Fa and SOC1R; Figure 4A). For this, we performed various PCR amplification cycles (28×, 32×, and 36×; Figure 2C) instead of employing real-time RT-PCR because the simultaneous quantification of two different products in a single PCR reaction was not realistic. Both the fully spliced 652-bp *SOC1* mRNA (SOC1T) and the ~770-bp higher molecular weight transcript (SOC1 variant; SOC1V) were increased in *elf9-1* compared with wild-type plants at 28 amplification cycles (28×; Figures 2C to 2E). The levels of SOC1T were higher in *elf9-1* than in wild-type plants at both 28× and 32×, but the difference was not obvious at 36× because the reactions were almost saturated (Figures 2C and 2D). We then compared the relative abundance of SOC1V versus SOC1T in the wild type and *elf9-1*. The relative abundance of SOC1V was higher in the mutant than in wild-type plants at all amplification cycles tested (Figure 2F). In summary, both the fully spliced *SOC1* mRNA (SOC1T) and the higher molecular weight variant

Figure 1. (continued).

their flowering times were determined as the number of rosette leaves present at bolting (leaf number). At least 10 individuals were scored for each genotype. Error bars represent SD.

(C) Schematic diagram of the genomic structure of *At5g16260*. The T-DNA insertion site in the *elf9-1* mutant is indicated. Gray boxes represent exons encoding two RRMs, and black boxes represent the other exons. Solid lines indicate introns. RRMs were predicted by SMART (http://smart.embl-heidelberg.de/).

(D) Genomic complementation of *elf9-1*. C1 indicates one of the *elf9-1* complementation lines containing a genomic *At5g16260* fragment (see text for details). Plants were grown for 75 d in SDs.

(E) Flowering time of three independent *elf9-1* complementation lines (C1, C2, and C3), as scored by the number of rosette leaves formed at bolting. Plants were grown in SDs, and the data presented are averages ± SD of at least 12 individuals for each genotype.

(F) Sequence comparison of the RRMs of ELF9, yeast CUS2, and human Tat-SF1. Each RRM is indicated by a solid line. The amino acid sequence alignment was generated using ClustalW (Thompson et al., 1994). Identical and similar amino acid residues are indicated by black and gray boxes, respectively.

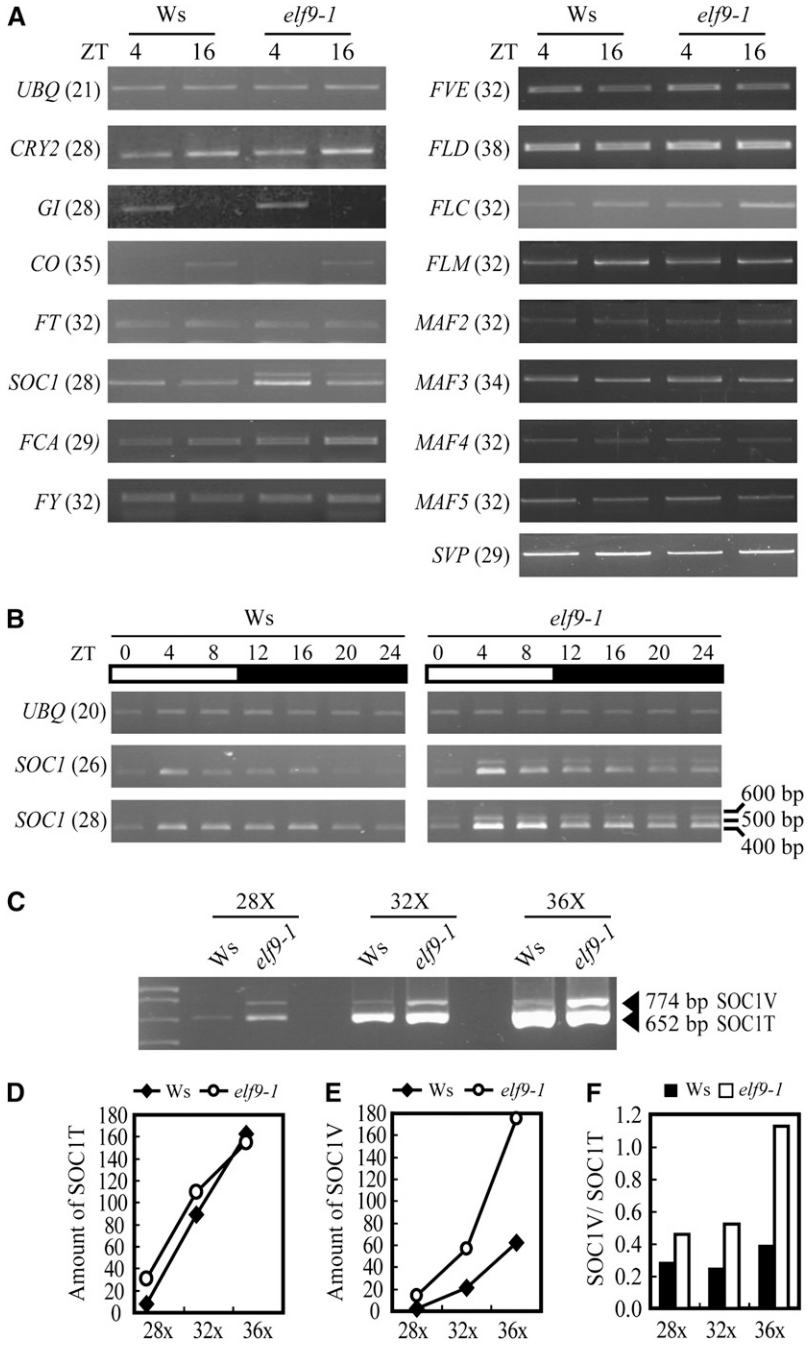

Figure 2. Elevated Expression of *SOC1* mRNA and Its Splicing Variant in *elf9-1*.

(A) Expression of flowering genes in *elf9-1*. Ws and *elf9-1* seedlings were grown under SD conditions for 15 d, harvested at ZT4 or ZT16, and used for RT-PCR analyses. *UBQ* was included as an expression control. The numbers in parentheses indicate amplification cycles (**[A]** and **[B]**). Identical results were obtained from two independent experiments, one of which is shown.

(B) Diurnal expression of the *SOC1* transcript in *elf9-1*. Seedlings were grown as in **(A)** and harvested every 4 h for RT-PCR analyses. SOC1F and SOC1R (Figure 4A; see Methods) were used to study *SOC1* expression. Identical results were obtained from two independent experiments, one of which is shown.

(C) Expression of full-length *SOC1* transcript and its splicing variant in *elf9-1*. RNAs isolated from the ZT4 seedlings in **(B)** were used for RT-PCR analyses employing SOC1Fa and SOC1R (Figure 4A; see Methods) as PCR primers, with the indicated number of PCR cycles.

(D) Quantification of SOC1T expression. SOC1T amplified from each genotype using the different PCR cycles in **(C)** was quantified and normalized based on the ZT4 *UBQ* in **(B)**. The *y* axis indicates the relative abundance of SOC1T. Closed diamonds indicate SOC1T abundance in the wild type; open circles indicate SOC1T in *elf9-1*.

SOC1 transcript (SOC1V) were increased as a consequence of the *elf9-1* mutation; however, SOC1V demonstrated a greater increase than SOC1T.

The simultaneous increase in both SOC1T and SOC1V in *elf9-1* led us to test the possibility that *SOC1* transcriptional activity is increased in *elf9-1* compared with the wild type. To assess this, we measured the association level of RNA Polymerase II (PolII) with the *SOC1* promoter using the chromatin immunoprecipitation (ChIP) assay with an RNA PolII-specific antibody, 8WG16, which can recognize both the unphosphorylated and hypo- and/or intermediately phosphorylated C-terminal heptapeptide repeat of RNA PolII (Stock et al., 2007). This antibody has been used to correlate RNA PolII binding with gene expression in a number of studies (e.g., Lee et al., 2006; Squazzo et al., 2006). Sets of primers spanning different regions of the *SOC1* promoter were used for the ChIP assay (Figure 3A). We first measured the association of RNA PolII with the *SOC1* promoter in *soc1-101D FRI* plants, which are known to possess much higher *SOC1* transcriptional activity than *FRI*-containing Columbia (Col *FRI*; Lee et al., 2000). Enhancement of RNA PolII binding to the *SOC1* promoter regions, SPR1 and SPR2, was observed in *soc1-101D FRI* compared with Col *FRI* (Figures 3B and 3D). The SPR3 promoter region was not amplified from *soc1-101D FRI* in the ChIP assay due to insertion of the activation-tagging T-DNA. No enrichment of RNA PolII binding in *soc1-101D FRI* compared with in Col *FRI* was observed in the SPR4 region, which is located several kilobases upstream of the *SOC1* start codon in *soc1-101D FRI* (Figures 3B and 3D). For *elf9-1*, there was no significant difference in RNA PolII association with the *SOC1* promoter regions compared with wild-type plants (Figures 3C and 3D). These data are consistent with a model in which ELF9 represses *SOC1* expression through a mechanism other than transcription.

SOC1V Is a *SOC1* Splicing Variant with an Unspliced Sixth Intron

To address the molecular nature of SOC1V, we gel-purified SOC1V (Figure 2C) and determined its sequence for the entire region. We found that SOC1V is a 774-bp, partially spliced *SOC1* transcript with an unspliced 6th intron (Figure 4A). We also sequenced SOC1T and, as expected, found it to be the fully spliced *SOC1* mRNA. SOC1V contains an in-frame translation termination codon (TGA) within the 6th intron, implying that SOC1V should encode a truncated SOC1 protein. To determine the specific abundance of SOC1V in the wild type versus *elf9-1*, we designed a primer (SOC6INT; Figure 4A) recognizing the 6th intron of *SOC1* and performed quantitative PCR (qPCR) analyses. The level of SOC1V was ~4- to 10-fold higher in *elf9-1* than in wild-type plants (Figure 4B).

In Figure 1, we show that the early flowering of *elf9-1* can be fully rescued by a genomic *At5g16260* construct. Because the *elf9-1* mutation led to increased levels of the two *SOC1* transcripts (SOC1T and SOC1V; Figure 2), we reasoned that those increases could also be rescued by the same genomic construct. To test this, the expression levels of the two *SOC1* transcripts were examined in two independent complementation lines. In the complementation lines, the increased expression levels of both SOC1T and SOC1V in *elf9-1* returned to the levels detected in the wild type (Figure 4C), demonstrating that the *elf9-1* mutation is indeed responsible for the increased expression of both SOC1T and SOC1V.

A mutation in the donor site of the 6th *SOC1* intron was recently reported (Lee et al., 2008). The *FRI*-containing *suppressor of soc1-101D 14* (*sso14*) mutant, which contains adenine instead of guanine in the first nucleotide position of the 6th *SOC1* intron, expressed a single truncated SOC1 protein and demonstrated a flowering phenotype intermediate between the extreme early flowering of *soc1-101D FRI* and the extreme late flowering of *SOC1 FRI* (Lee et al., 2008). In the *SOC1* activation-tagged *soc1-101D FRI*, a high level of SOC1T and a low level of SOC1V were detected by RT-PCR (see Supplemental Figure 3 online). In *sso14*, four different forms of *SOC1* transcript were amplified by the primers used in Figure 2C (see Supplemental Figure 3 online). However, it was not clear which splicing variants contribute to the partial *SOC1* activity in *sso14* because each of the four splicing variants present in *sso14* could theoretically result in different degrees of SOC1 protein truncation. We were also not able to conclude whether the truncated SOC1 protein encoded by SOC1V has partial activity based on the analysis of *sso14*.

Early Flowering of *elf9-1* Is Likely Due to Increased Expression of *SOC1*

In our study using a variety of flowering genes, *SOC1* was unique in having increased steady state transcript levels in *elf9-1* mutants compared with the wild type (Figure 2A). This raised the possibility that the increased expression of *SOC1* is responsible for the early flowering of *elf9-1*. To test this possibility, we crossed *elf9-1* with *soc1-2* (Moon et al., 2003), which are in the Ws and Col accessions, respectively. Because these two accessions differ in their flowering time behavior, we generated a large F2 population from the cross, genotyped, and directly measured flowering time for segregating each genotype (Figure 5). When wild-type Col and Ws plants flowered, each with 12 to ~13 and 7 to ~8 rosette leaves, respectively, *soc1-2* flowered with 22 to ~23 rosette leaves, and *elf9-1* flowered with ~6 rosette leaves. In the F2 population, the *elf9-1* single homozygous mutants and the *soc1-2* single homozygous mutants

Figure 2. (continued).

(E) Quantification of SOC1V expression. Quantification and normalization were performed as in **(D)**.

(F) A greater increase in SOC1V than in SOC1T was observed in *elf9-1* than in the wild type. Each quantity of SOC1V in **(E)** was divided by the corresponding quantity of SOC1T in **(D)**, and the values were plotted on the *y* axis. Closed boxes represent the SOC1V/SOC1T ratios in the wild type; open boxes represent those in *elf9-1*.

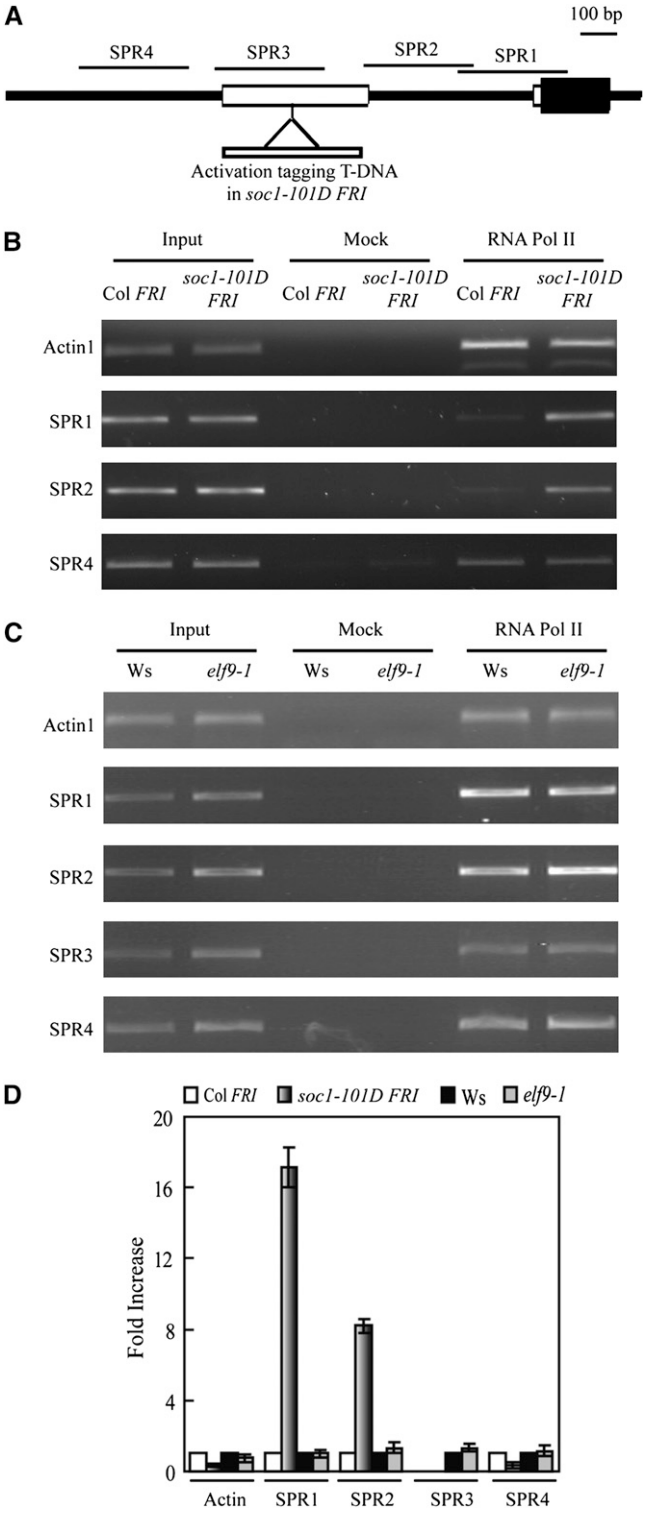

Figure 3. *SOC1* Transcriptional Activity Is Not Altered by the *elf9-1* Mutation.

(A) *SOC1* promoter regions evaluated with the ChIP assay. The larger white box represents the first exonic 5′ UTR, and the smaller white box represents the second exonic 5′ UTR. The transcribed region within the second exon is indicated by the black box. Labeled lines indicate promoter regions amplified by primers (see Methods) during the ChIP assay. The location of the activation-tagging T-DNA inserted in *soc1-101D FRI* (Lee et al., 2000) is marked below the first exonic 5′ UTR.

(B) ChIP assay of *SOC1* chromatin with RNA PolII-specific antibody using Col *FRI* and *soc1-101D FRI* plants. "Input" indicates chromatin before immunoprecipitation. "Mock" refers to control samples lacking antibody. *Actin1* was used as an internal control.

(C) ChIP assay of *SOC1* chromatin with RNA PolII-specific antibody using wild-type Ws and *elf9-1* plants.

(D) qPCR analysis of ChIP assays in **(B)** and **(C)**. The levels of Col *FRI* and wild-type Ws were set to 1 after normalization against input chromatin. Error bars represent SD of three technical replicates.

flowered with 7 to ~8 and ~17 rosette leaves, respectively. However, the *soc1-2 elf9-1* double homozygous mutants flowered at about the same time as the *soc1-2* single mutants, with 17 to ~18 rosette leaves. Thus, *soc1-2* was fully epistatic to *elf9-1*, suggesting that the early flowering observed for *elf9-1* was caused by the increased expression of *SOC1* in the mutant.

Constitutive Overexpression of *ELF9* Rescues the *elf9-1* Mutant Phenotype but Does Not Cause Additional Effects

Loss of *ELF9* activity in *elf9-1* resulted in increased SOC1T and SOC1V expression, culminating in early flowering (Figures 2, 4, and 5). Consequently, we evaluated the effect of *ELF9* overexpression (OE) on both flowering time and *SOC1* expression. We generated an *ELF9OE* construct using the *CaMV35S* promoter, *MYC* tag, and full-length genomic *ELF9* and introduced this construct into wild-type Ws. Two representative transgenic lines (*MycELF9OE1* in Ws and *MycELF9OE2* in Ws) demonstrating robust ELF9 mRNA expression were selected and crossed with the *elf9-1* mutants.

The phenotype of *MycELF9OE1* and *MycELF9OE2* in Ws or homozygous *elf9-1* mutants was identical to that of wild-type Ws plants (see Supplemental Figure 4A online). All these transgenic plants demonstrated elevated levels of *ELF9* mRNA expression compared with those detected in wild-type Ws (see Supplemental Figure 4B online), although the expression levels of SOC1T and SOC1V were approximately the same (see Supplemental Figure 4B online). In particular, the increased expression of SOC1T and SOC1V in *elf9-1* was fully rescued by overexpression of *ELF9* in the *elf9-1* mutant background.

Consistent with the rescue of SOC1T and SOC1V expression, the flowering times of the *MycELF9OE*s in Ws and *elf9-1* were not significantly different from those of wild-type Ws both in LDs (see Supplemental Figure 4C online) and SDs (see Supplemental Figure 4D online). Therefore, overexpression of *ELF9* rescued the early flowering of *elf9-1* caused by differential *SOC1* expression but did not delay flowering or induce additional morphological phenotypes.

Direct Binding of ELF9 to *SOC1* Transcript

All the molecular and genetic data presented above suggest that ELF9 might be involved in the processing of *SOC1* pre-mRNA.

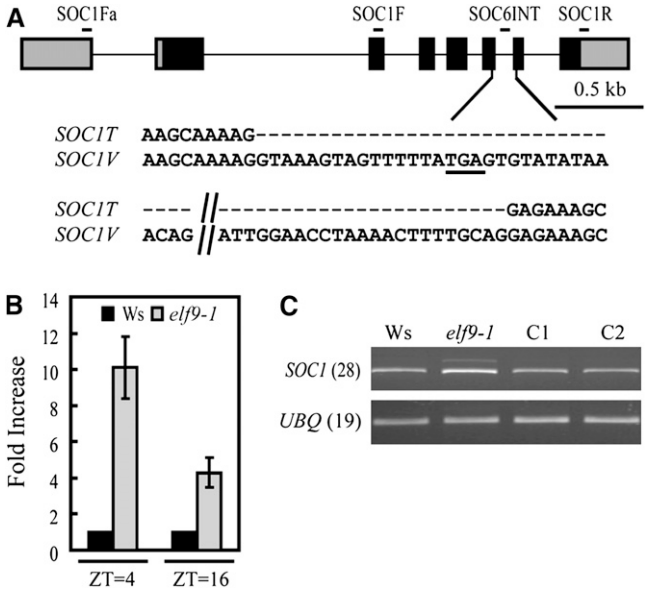

Figure 4. SOC1V Contains the Unspliced Sixth Intron of *SOC1*.

(A) Schematic representation of the *SOC1* genomic region and alignment of SOC1T and SOC1V sequences around the 6th intron region, which is retained in SOC1V. The premature in-frame termination codon within SOC1V is underlined. The gray boxes in the front indicate exonic 5′ UTRs, and the rear gray box represents the 3′ UTR. The primers used for the RT-PCR analyses shown in Figures 2 and 4 are indicated.

(B) Increased level of SOC1V in *elf9-1*, as measured by qPCR. SOC6INT, which is specific to the 6th intron of *SOC1*, and SOC1Fa were used for the specific detection of SOC1V. The wild-type Ws levels were set to 1 after normalization against *UBQ* expression. Error bars represent SD of three technical replicates.

(C) Complementation of the increased expression of SOC1T and SOC1V in *elf9-1* with genomic *At5g16260*. C1 and C2 are the two transgenic lines described in Figure 1E. Seedlings were grown in SD as described in Figure 2A and used for RNA isolation (**[B]**and **[C]**). The seedlings were harvested at ZT4. The numbers in parentheses indicate amplification cycles.

Since ELF9 is an RRM-containing protein, it could play a direct role in *SOC1* pre-mRNA processing. To test this hypothesis, RT-PCR was performed after immunoprecipitation (IP-RT-PCR; Wang et al., 2008) using the *MycELF9OE1* and *MycELF9OE2* in *elf9-1* plants. After immunoprecipitation with Myc-specific antibody, RT was performed using a reverse primer specific to the 7th exon of *SOC1* (SOC1EX7R; Figure 6A) in the presence [(+) RT] or absence [(−) RT] of reverse transcriptase. PCR was then performed using primers designed to recognize various positions along the *SOC1* pre-mRNA (Figures 6A and 6B).

First, binding signals were enriched in the SIT3 region of the *MycELF9OE1* and *MycELF9OE2* plants only in the presence of reverse transcriptase (Figure 6B). Because an ~500-bp fragment is expected to be amplified either from genomic DNA (as for the Input; Figure 6B) or from fully unspliced *SOC1* pre-mRNA, the 162-bp band specifically enriched in the *MycELF9OE1* and *MycELF9OE2* plants after IP-RT-PCR is expected to be a product of the spliced SOC1 transcript that lacks the 3rd and 4th introns. Second, binding signal enrichment was also obtained for the SIT4 region of the *MycELF9OE1* and *MycELF9OE2* plants (Figure 6B). Unlike SIT3, for which both the forward and reverse primers were designed to bind exonic regions, the SIT4 reverse primer was designed to recognize a sequence in the 6th intron that is retained in SOC1V. Therefore, the 277-bp SIT4 band would have been amplified from a partially spliced *SOC1* transcript containing the 6th intron but not the 3rd, 4th, and 5th introns. Considering that SOC1V was found to be the unique splicing variant, even after extensive RT-PCR amplifications (Figure 2C), enrichment of the 277-bp SIT4 band in the *MycELF9OE1* and *MycELF9OE2* plants after IP-RT-PCR might indicate that SOC1V is a binding target of ELF9. Therefore, the binding enrichments in the SIT3 and SIT4 regions of the *MycELF9OE1* and *MycELF9OE2* plants in these IP-RT-PCR analyses suggests that SOC1V, but not the fully unspliced *SOC1* pre-mRNA, is the preferential binding target of ELF9.

The lack of enrichment in the SIT1 and SIT2 regions was probably due to the lower production efficiency of the full-length *SOC1* cDNA compared with shorter *SOC1* cDNAs during reverse transcription. Alternatively, the full-length *SOC1* transcript could be more vulnerable than shorter forms of the transcript to residual nuclease attack during the prolonged immunoprecipitation period used for IP-RT-PCR. The use of SOC1EX7R instead

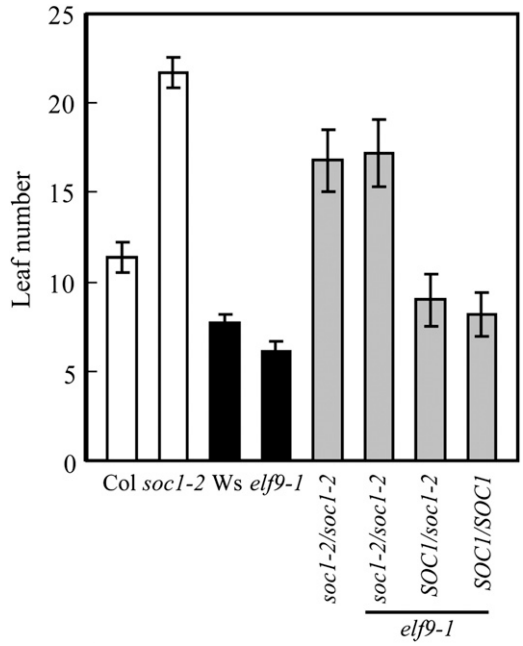

Figure 5. Genetic Interaction between *SOC1* and *ELF9*.

To measure the flowering time of the *soc1-2 elf9-1* double mutant and compare it with those of *soc1-2* (Col accession background; white bars) and *elf9-1* (Ws accession background; black bars) single mutants, individuals in the segregated F2 population obtained by crossing *soc1-2* and *elf9-1* (gray bars) were directly genotyped and evaluated for changes in flowering time under LD conditions. Flowering time was determined as the number of rosette leaves present at bolting. Error bars indicate SD of at least 10 individuals for each genotype.

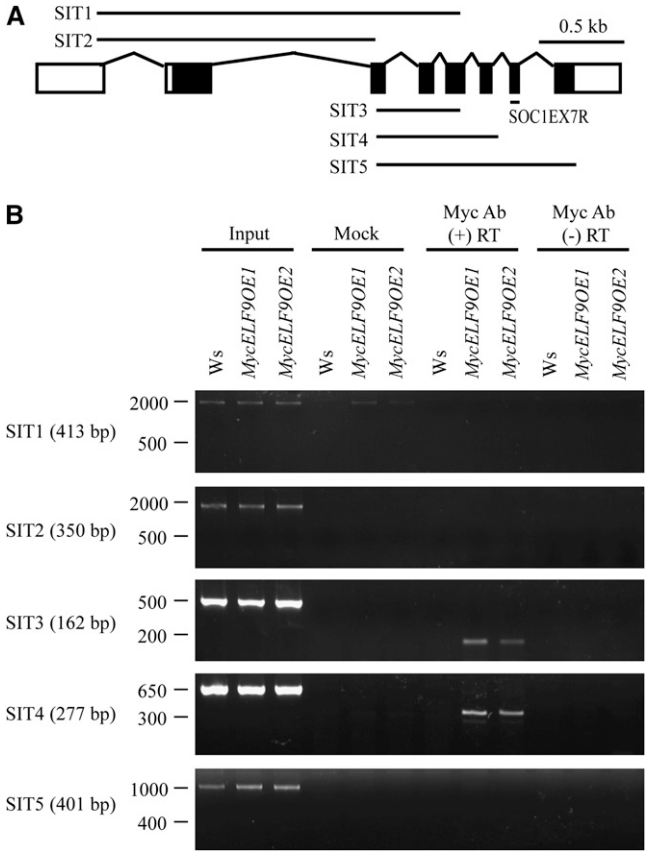

Figure 6. ELF9 Protein Binds *SOC1* Transcript.

(A) Schematic diagram of *SOC1* pre-mRNA showing regions amplified by the primers (see Methods) used for IP-RT-PCR analysis. The two white boxes in the front represent the 5′ UTR, while the white box at the end indicates the 3′ UTR. Introns are represented by thin lines between the exons. Primer SOC1EX7R indicated below the 7th exon was used instead of an oligo(dT) primer for RT in this experiment.

(B) ELF9 binding to *SOC1* transcript. Fifteen-day-old transgenic seedlings harboring the *CaMV35S*$_{pro}$*:Myc:ELF9* fusion construct were harvested and immunoprecipitated with Myc-specific antibody. RT was performed using the eluates with SOC1EX7R as a primer (see Methods). Input: chromatin before immunoprecipitation. Mock: control samples lacking antibody. Myc Ab (+) RT: reverse transcribed with reverse transcriptase after immunoprecipitation with Myc antibody. Myc Ab (−) RT: reverse transcribed without reverse transcriptase after immunoprecipitation with Myc antibody.

of an oligo-(dT) primer in the RT reaction did not allow for conversion of the 8th exon, which is recognized by the reverse primer for SIT5, into cDNA. Thus, SIT5 served as an additional control, along with (−)RT, demonstrating that SIT3 and SIT4-enriched signals were derived specifically from *SOC1* transcript.

ELF9 Is Required for NMD in *Arabidopsis*

In the *elf9-1* mutants, the levels of both SOC1T and SOC1V were increased without enhanced association of RNA PolII with *SOC1* chromatin (Figures 2 and 3), and ELF9 protein bound directly to the SOC1V-like partially spliced *SOC1* transcript, which lacks the 3rd, 4th, and 5th introns but contains the 6th intron (Figure 6). These results indicate that ELF9 participates in *SOC1* expression at a posttranscriptional level and led us to speculate about three scenarios regarding the biochemical role of ELF9: namely, (1) in *SOC1* splicing, (2) in the transport of *SOC1* transcript from the nucleus to the cytoplasm, and (3) in NMD. However, the first two scenarios are not consistent with the simultaneous increase of both SOC1T and SOC1V in *elf9-1* mutants.

The third scenario presents a possible role for ELF9 in NMD, which is a system for degrading abnormal transcripts with PTCs (Isken and Maquat, 2008). SOC1V is an abnormal *SOC1* transcript with a PTC (Figure 4A) and thus might be a target for NMD. The increased level of SOC1V in *elf9-1* mutants is consistent with this scenario. Furthermore, several wild-type mRNAs are known to be upregulated in NMD mutants. These include certain yeast mRNAs encoding telomerase components or regulators (Dahlseid et al., 2003), *CPA1* mRNA (Ruiz-Echevarria and Peltz, 2000), and *SPT10* mRNA (Welch and Jacobson, 1999). *CPA1* mRNA is degraded by NMD because of an upstream open reading frame that leads to a PTC. *SPT10* mRNA becomes an NMD target since ribosomes often scan beyond the initiator AUG and initiate at the next downstream AUG (leaky scanning), resulting in premature translation termination. Sequence analyses of the *SOC1* 5′ UTR and coding region revealed multiple candidate initiator codons for leaky scanning as well as upstream open reading frame candidates (see Supplemental Figure 5 online). Therefore, we considered the possibility that not only SOC1V, but also wild-type *SOC1* mRNA (SOC1T), are regulated by NMD and that the expression of both of these transcripts are increased in NMD mutants.

Although the molecular mechanism of NMD in *Arabidopsis* is not known, the genetic functions of *Arabidopsis* homologs of upframeshift (UPF) 1 and 3, which are evolutionarily conserved key components of NMD in yeast and animals, have been addressed (Hori and Watanabe, 2005; Arciga-Reyes et al., 2006). These studies have shown that several transcripts containing PTCs are upregulated in the *Arabidopsis upf1* and *upf3* mutants. Therefore, as a first step to determining whether ELF9 is involved in NMD in *Arabidopsis*, we examined the expression levels of five of these PTC-containing *Arabidopsis* transcripts (Figure 7A) in wild-type and *elf9-1* plants and in one of the *elf9-1* complementation lines. Among the PTC-containing transcripts examined, those of *AGL88*, *At1g10160*, *At1g66710*, and *At3g63340* were upregulated in *elf9-1*, and their increased expression was rescued by the *ELF9* genomic construct (Figure 7B). However, neither the PTC-containing At5g62760b transcript nor the At5g62760a transcript, which does not contain a PTC, yielded detectable differences between the wild type and *elf9-1* at two different amplification cycles in our RT-PCR analysis. These transcripts obtained from Ws plants had exactly the same sequences as those from Col plants, and the At5g62760b transcript contained the PTC.

Next, we performed IP-RT-PCR to test whether the increase of the PTC-containing transcripts in *elf9-1* is directly mediated by ELF9 protein. As shown in Figure 7C, three of the four transcripts that were increased in *elf9-1* were also enriched in the

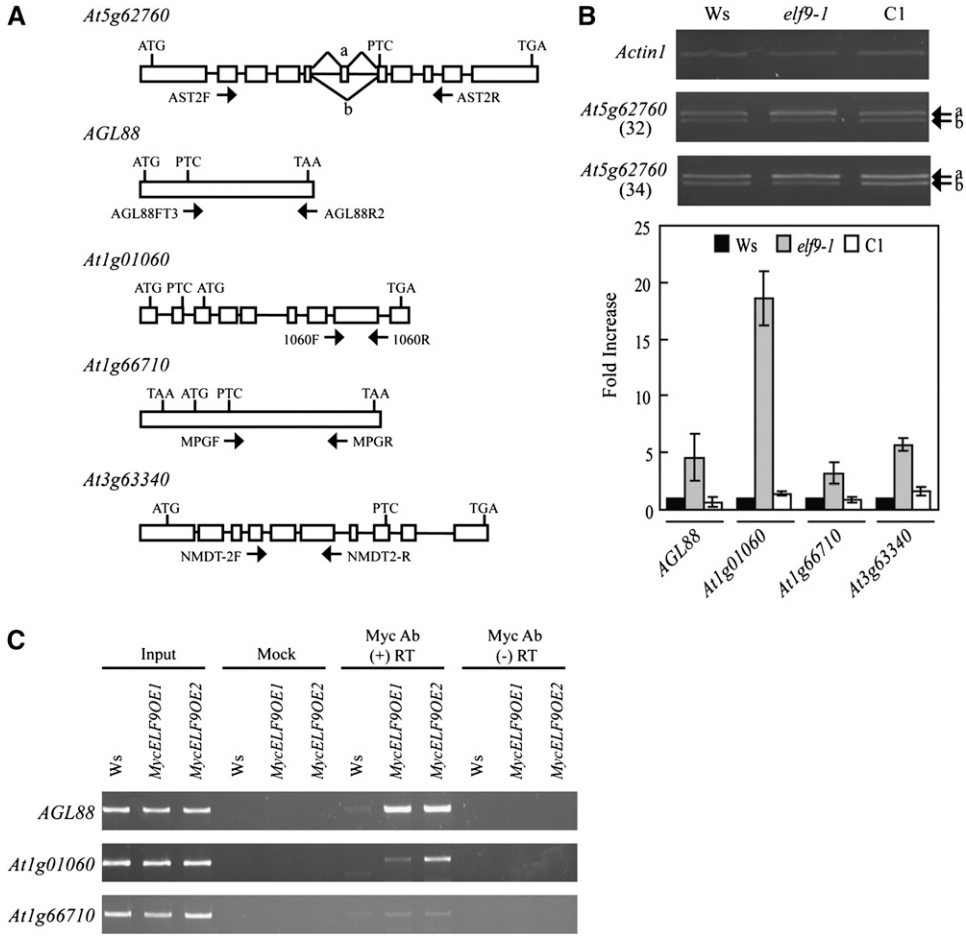

Figure 7. Increased Expression of NMD Target Transcripts in *elf9-1*.

(A) Schematic diagrams of the five PTC-containing genes (adopted from Hori and Watanabe, 2005; Arciga-Reyes et al., 2006) tested for NMD in *elf9-1*. ATGs indicate translation start codons, while TGAs or TAAs represent stop codons. Exons are indicated by boxes and introns by lines. The PTC site for each gene is marked. Arrows indicate the positions of the RT-PCR primers. The "a" and "b" indicate two alternatively spliced transcripts of *At5g62760*, namely, At5g62760a and At5g62760b, respectively.

(B) RT-PCR or qPCR analysis of the PTC-containing genes shown in **(A)**. The same RNAs used in Figure 4C were evaluated. C1 is one of the *elf9-1* complementation lines described in Figures 1D, 1E, and 4C. *Actin1* was used as an expression control. The numbers in parentheses indicate amplification cycles for RT-PCR analysis. The wild-type Ws levels were set to 1 after normalization against *Actin1* for qPCR analysis. Error bars represent SD of three technical replicates.

(C) ELF9 binding to the PTC-containing transcripts shown in **(B)**. RNAs immunoprecipitated with Myc-specific antibody and purified (shown in Figure 6B) were reverse transcribed with an oligo(dT) primer. PCR was performed with the primers used in Figure 7B. Figure captions are as described in Figure 6B.

MycELF9OE1 and *MycELF9OE2* plants analyzed by IP-RT-PCR. The enrichment occurred only after reverse transcription, indicating that ELF9 binds specifically to RNAs of these genes. In the case of the *At3g63340* transcript, enrichment could not be determined precisely because of the amplification of multiple nonspecific bands.

We could isolate another T-DNA insertion allele of *ELF9* in the Col accession (*elf9-2*; Figure 8A) from the SALK T-DNA collection. Unlike *elf9-1*, which is in the Ws background, *elf9-2* mutants displayed a number of abnormal morphological phenotypes, such as reduced fertility, smaller leaf size, and elongated leaf morphology (Figure 8A). These phenotypes were similar to those caused by some *upf1* and *upf3* mutant alleles (Arciga-Reyes et al., 2006). As in *elf9-1*, transcript levels of *SOC1* (SOC1T), *AGL88*, *At1g66710*, and *At3g63340* were elevated in *elf9-2* compared with in wild-type Col (Figures 8B and 8C). Levels of At5g62760a and At5g62760b transcripts were not significantly altered by the *elf9-2* mutation (Figure 8B), as was the case for *elf9-1* (Figure 7B). However, unlike in *elf9-1* and wild-type Ws, expression of SOC1V was not detected in *elf9-2* or in wild-type Col even after extensive PCR (Figure 8B). Therefore, loss of ELF9 activity in the Col background results in the increased expression

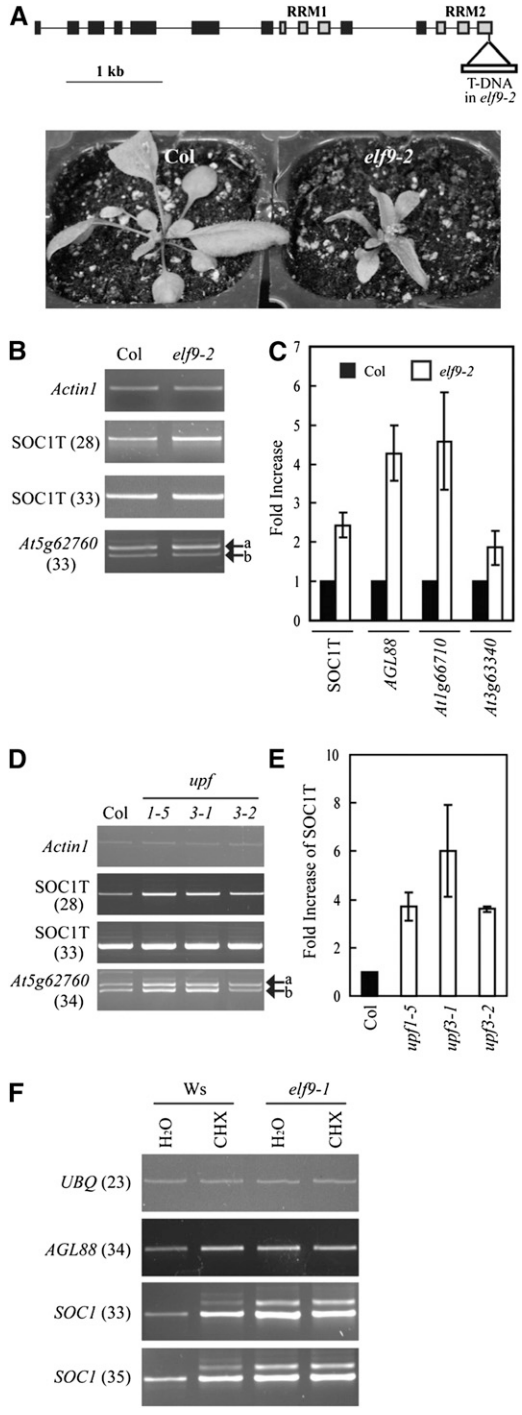

Figure 8. Increased Expression of SOC1T in *elf9-2* and *upf* Mutants and by CHX.

(A) Schematic diagram of the genomic structure of *ELF9* and the phenotypes of *elf9-2*. The T-DNA insertion site in the *elf9-2* mutant is indicated. Schematic is as described in Figure 1C. Wild-type Col and the *elf9-2* mutant plants were grown for 28 d in LDs.

(B) RT-PCR analysis of *SOC1* and *At5g62760* expression in *elf9-2*. Col and *elf9-2* plants were grown in LDs for 28 d, harvested at ZT8, and used for RNA extraction. SOC1Fa and SOC1R were used as PCR primers to amplify *SOC1* (**[B]** to **[F]**). *Actin1* was included as an expression control. Identical results were obtained from two independent experiments, one of which is shown.

(C) qPCR analysis of the PTC-containing genes. The same RNAs used in **(B)** were evaluated. The wild-type Col levels were set to 1 after normalization against *Actin1* for qPCR analysis. Error bars represent SD of three technical replicates.

(D) RT-PCR analysis of *SOC1* and *At5g62760* expression in *upf1-5*, *upf3-1*, and *upf3-2* mutants. The wild-type Col, *upf1-5*, *upf3-1*, and *upf3-2* plants were grown in LDs for 20 d, harvested at ZT8, and used for RNA extraction. *Actin1* was included as an expression control. Identical results were obtained from two independent experiments, one of which is shown.

(E) qPCR analysis of SOC1T expression. The same RNAs used in **(D)** were evaluated. The wild-type Col levels were set to 1 after normalization against *Actin1* for qPCR analysis. Error bars represent SD of three technical replicates.

(F) Increased expression of *SOC1* transcripts by CHX treatment. See Methods for details. *UBQ* was included as an expression control. Identical results were obtained from two independent experiments, one of which is shown.

of SOC1T, as is the case in the Ws background. Production of SOC1V, which is a *SOC1* splicing variant with an unspliced 6th intron, is much lower in the Col accession than in Ws, possibly due to more efficient splicing of the 6th intron in Col.

If the *SOC1* transcript is regulated by NMD, it might also be affected by the mutations in the core NMD components, namely, UPF1 and UPF3. Consistent with this hypothesis, SOC1T expression was increased by one *upf1* (i.e., *upf1-5*) mutation and two *upf3* mutations (i.e., *upf3-1* and *upf3-2*; Figures 8D and 8E). As in *elf9-2* (Figure 8B), expression of SOC1V was not detected either, even after extensive PCR in these *upf* mutants (Figure 8D). Although the expression of At5g62760b, but not of the At5g62760a transcript, was reported to be increased in *upf1-5* (Arciga-Reyes et al., 2006), both of these transcripts showed increased expression in *upf1-5* and *upf3-1* mutants, relative to the wild type, in our assay (Figure 8D). Since NMD is initiated by the recognition of PTC during translation, cycloheximide (CHX) is often used as an NMD inhibitor (Carter et al., 1995; Hori and Watanabe, 2005). When we treated leaf sections of wild-type Ws and *elf9-1* plants with CHX (Figure 8F), the expression of one of the known PTC-containing transcripts, *AGL88*, was increased in the wild type but not in *elf9-1*. Both SOC1T and SOC1V levels were also elevated in the wild type but not in *elf9-1* after the CHX treatment, which is consistent with our other results showing that *SOC1* transcripts are regulated by ELF9-mediated NMD.

In summary, ELF9 is believed to be involved in NMD in *Arabidopsis* for a subset of PTC-containing transcripts, including those of *SOC1* and of the genes tested above. In the process, the RRM protein ELF9 might provide some degree of target specificity for the NMD machinery composed of UPF1, UPF3, and other unknown factors.

DISCUSSION

Integration of environmental cues with endogenous and developmental components occurs via numerous genes acting in an

intricate network that controls flowering time in plants (reviewed in Searle and Coupland, 2004; Sung and Amasino, 2005; Bäurle and Dean, 2006). This regulatory network includes transcriptional regulation, mRNA processing, and protein turnover. However, there have been few reports on the role of RNA processing in the regulation of flowering time. *ABA HYPERSENSITIVE1* (*ABH1*), which encodes the large subunit of the nuclear mRNA cap binding complex, causes early flowering in response to both SD and LD when mutated (Hugouvieux et al., 2001; Bezerra et al., 2004). *ABH1* is required for high expression levels of *FLC* and *FLM* mRNAs (Bezerra et al., 2004; Kuhn et al., 2007), and there was an accumulation of a partially spliced *FLC* transcript with the 1st intron in the *abh1* mutants (Kuhn et al., 2007). However, it has not been demonstrated whether the differential expression of *FLC* and *FLM* transcripts in *abh1* is a direct consequence of the loss of ABH1 activity. *HUA2* was first known to play a role in the efficient splicing of intron 2 in *AGAMOUS* pre-mRNA (Cheng et al., 2003; Chen and Meyerowitz, 1999) and was later reported to also be required for high expression levels of *FLC*, *FLM*, *MAF2*, and *SVP* mRNAs but not for *SOC1* mRNA (Doyle et al., 2005). The biochemical role of HUA2 during mRNA expression of these *FLC* family MADS genes remains elusive. One of the RRM protein-encoding genes functioning as an *FLC* repressor in the autonomous pathway, *FCA*, has been shown to regulate its own expression in an *FY*-dependent manner by promoting the use of an internal polyadenylation site in the *FCA* transcript (Macknight et al., 2002; Quesada et al., 2003). However, more recently, FCA was shown to act through FLD with respect to chromatin modification and transcriptional regulation of *FLC* rather than by affecting *FLC* mRNA processing (Liu et al., 2007).

SOC1 expression is regulated primarily by the negative and positive effect on *SOC1* transcription exerted by FLC and CO, respectively. SVP is another negative regulator of *SOC1* that may be part of a repressive FLC protein complex (Li et al., 2008). Other positive regulators of *SOC1* include AGL24 (Liu et al., 2008a), GA (Moon et al., 2003), and the FT-FD complex in the shoot apex, possibly via an indirect mechanism (Wigge et al., 2005).

In this study, we showed that loss of ELF9, an RRM protein, affects *Arabidopsis* flowering time possibly through altering NMD of the *SOC1* transcript. The *elf9-1* mutants flowered early, especially in SDs (Figures 1A and 1B), and this early flowering was associated with increased expression of *SOC1* transcript (Figure 2A). Furthermore, the late flowering of *soc1* was fully epistatic to *elf9-1*–induced early flowering (Figure 5), demonstrating that the early flowering of *elf9-1* mutants is caused primarily or specifically by the increased expression of *SOC1* transcript. ELF9 protein can directly bind a partially spliced *SOC1* transcript (Figure 6), resulting in posttranscriptional turnover possibly through NMD (Figures 2, 4, 7, and 8). Therefore, ELF9 allows for a previously unknown layer of regulation of *SOC1* expression.

As discussed below, we believe the most likely role of ELF9 in modulating *SOC1* mRNA levels is via NMD. Our data are not consistent with a role in *SOC1* splicing or transport of the *SOC1* transcript from the nucleus to cytoplasm. The ELF9-mediated posttranscriptional regulation of *SOC1* might be a part of the general NMD-dependent mRNA quality control system in *Arabidopsis*, due to the following reasons. First, multiple known *Arabidopsis* NMD target transcripts are the binding targets of ELF9 and are increased in the *elf9* mutants (Figures 7B, 7C, and 8C). Second, *SOC1* transcripts are also increased in the mutants of NMD core components (Figure 8E) and by CHX treatment (Figure 8F). However, the expression of at least one of the NMD target genes, *At5g62760*, was not increased in *elf9*, suggesting that, unlike evolutionarily well-conserved NMD factors like UPF1 and UPF3, RNA binding components of the NMD machinery might have some degree of target specificity and be involved in selecting target transcripts during the initial stage of NMD. Nonetheless, although *SOC1* was the only target among flowering genes examined (Figure 2), ELF9 clearly targets other transcripts. In animals and yeast, ~3 to 10% of the transcriptome is believed to be either direct or indirect targets of NMD (Lelivelt and Culbertson, 1999; Ni et al., 2007).

The Ws allele (*elf9-1*) and the Col allele (*elf9-2*) showed differences in phenotype and in the generation of SOC1V. Although the expression of *At1g66710* showed a higher fold increase in *elf9-2* than in *elf9-1* compared with each wild type, the expression of *At3g63340* was increased more in *elf9-1* than in *elf9-2* (Figures 7B and 8C). Furthermore, the 6th intron of *SOC1* displayed a much lower splicing efficiency than the other introns in Ws but not in Col plants (Figures 2C, 8B, and 8D). The lower splicing efficiency of the 6th intron of *SOC1* was observed more clearly when *SOC1* was overexpressed in wild-type Ws plants (see Supplemental Figure 6 online). In the Col background, SOC1V was detected at a low level only in a genetic background inducing an extremely high level of *SOC1* transcription (Col with *soc1-101D FRI* genotype; see Supplemental Figure 3 online). Therefore, we believe it is likely that the differences in phenotype and the generation of SOC1V between *elf9-1* and *elf9-2* are ecotype dependent and not due to allele strength.

NMD has been extensively studied in yeast and mammalian cells (reviewed in Isken and Maquat, 2008; Shyu et al., 2008). Cells routinely make mistakes due to the inefficiency or inaccuracy of RNA metabolic processes. It is important for cells to eliminate mRNAs that contain PTC since the resulting truncated proteins have the potential to be nonfunctional or acquire dominant-negative or gain-of-function activities. Therefore, NMD provides an important means by which cells ensure the quality of proteins produced (Isken and Maquat, 2008; Shyu et al., 2008). Mammals use machinery and mechanisms that differ from those present in yeast. In yeast, an abnormally long distance between the termination codon and 3′ poly(A) tail, as defined by the presence of poly(A) binding protein 1, seems to be sufficient to elicit NMD, whereas in mammals, NMD usually requires at least one intron within the pre-mRNA that results in the deposition of a post-splicing exon-junction complex (EJC) of proteins situated more than ~25 to 30 nucleotides downstream of the termination codon (Isken and Maquat, 2008). Despite numerous differences, the two systems use several common components, such as UPF1, UPF2, and UPF3. Based on such evolutionary conservation, the in vivo functions of the homologs of a few common NMD components have been studied in plants. *Arabidopsis* homologs of UPF1 and UPF3 have been shown to be required for NMD of PTC-containing mRNAs transcribed from both intron-containing and intronless genes (Hori and Watanabe, 2005; Arciga-Reyes

et al., 2006). This study shows that ELF9 is also required for NMD of both intron-containing (*At1g01060* and *At3g63340*) and intronless (*AGL88* and *At1g66710*) transcripts (Figure 7). Therefore, unlike mammalian NMD, which relies entirely on EJC, plant NMD surveillance systems may recognize both spliced and unspliced transcripts or rely on both EJC-dependent and independent mechanisms.

The biochemical mechanisms responsible for NMD in plants remain elusive, and there have been no previous reports on protein complexes that mediate NMD in plants. Although NMD is finally executed within the cytoplasm, assembly of the protein complex for NMD is initiated within the nucleus after splicing of the target transcript in mammals. Consistent with this, some proteins that function in NMD are preferentially localized in the nucleus, while others are in the cytoplasm. Many of these proteins are also able to shuttle between the nucleus and cytoplasm (reviewed in Isken and Maquat, 2008). Preferential localization of the ELF9:GFP fusion protein in the nucleus (see Supplemental Figure 1 online) suggests that ELF9 might function during the early stages of NMD, possibly during the initial assembly of the protein complex for NMD. Our observation that ELF9 binds a partially spliced *SOC1* transcript retaining the PTC-containing 6th intron, but not the 3rd, 4th, and 5th introns (Figure 6), is consistent with this possibility. Perhaps ELF9 recognizes PTC-containing aberrant transcripts and initiates assembly of the NMD protein complex. Whether ELF9 moves out of the nucleus into the cytoplasm as a component of the complex at later stages has yet to be determined. It is possible that a small fraction of ELF9 bound to transcripts destined for NMD moves from the nucleus into the cytoplasm and finally shuttles back into the nucleus. Because the ELF9:GFP fusion protein shown in Supplemental Figure 1 online was driven by the strong constitutive *CaMV35S* promoter, the free form of the fusion protein might have been easily detected within the nucleus, while the small fraction representing the substrate-bound form, potentially shuttling between the nucleus and cytoplasm, was barely detected. Hence, the subcellular localization and the possibility of the ELF9 protein shuttling between the nucleus and cytoplasm require further investigation.

ELF9 is a single-copy gene in the *Arabidopsis* genome. Database searches for proteins with >80% amino acid similarities to ELF9 in regions containing the two RRMs revealed a single ELF9 homolog in rice (*Oryza sativa*) and two homologs in sorghum (*Sorghum bicolor*) and poplar (*Populous trichocarpa*; see Supplemental Figure 7 online and http://www.phytozome.net/). Therefore, a role for ELF9 is likely to be conserved in higher plants.

METHODS

Plant Materials and Growth Conditions

The *elf9-1* mutant was isolated from an activation-tagging T-DNA insertion population constructed in the Ws background. The two mutants that were in the Col background, *soc1-2* (Moon et al., 2003) and *soc1-101D FRI* (Lee et al., 2000), have been previously described. The *elf9-2* T-DNA insertion mutant in the Col background (SALK_040796) was obtained from the SALK collection (http://signal.salk.edu/). For RT-PCR, surface-sterilized seeds were sown on MS media (Murashige and Skoog, 1962) containing 1% sucrose, maintained in the dark at 4°C for 2 d, and then transferred to 22°C. All plants were grown under ~100 μE m^{-2} s^{-1} cool white fluorescent light at 22°C.

T-DNA Flanking Sequence Analyses

The sequence flanking the T-DNA of *elf9-1* was obtained using thermal asymmetric interlaced PCR (Liu et al., 1995) as described by Schomburg et al. (2003). The T-DNA border of *elf9-1* was defined by sequencing PCR products obtained using a T-DNA border primer (JL270: 5′-TTTCTCCATATTGACCATCATACTCATTG-3′) and gene-specific primers. SALKLB1 (5′-GCAAACCAGCGTGGACCGCTTGCTGCAACT-3′) was used as a T-DNA border primer for *elf9-2*.

ChIP Assays

ChIP was performed as described by Han et al. (2007) using 14- to 16-d-old seedlings. Briefly, seedlings were vacuum infiltrated with 1% formaldehyde for cross-linking and ground in liquid nitrogen after quenching the cross-linking process. Chromatin was isolated and sonicated into ~0.5- to 1-kb fragments. RNA PolII-specific monoclonal antibody (8WG16; Covance) was added to the chromatin solution, which had been precleared with salmon sperm DNA/Protein A agarose beads (Upstate Biotechnology). After subsequent incubation with salmon sperm DNA/Protein A agarose beads, immunocomplexes were precipitated and eluted from the beads. The cross-links were reversed, and residual proteins in the immunocomplexes were removed by incubation with proteinase K, followed by phenol/chloroform extraction. DNA was recovered by ethanol precipitation. The amount of immunoprecipitated *SOC1* chromatin was determined by evaluating four different regions of the *SOC1* promoter by PCR. The sequences of the primer pairs used for each PCR reaction were as follows: SPR1, PF1 (5′-GGGTACTTAATCTTTCGTTGAC-3′) and PR1 (5′-CTTGTCTGCTTGTTGCATTCTC-3′); SPR2, SOC1Fa (5′-CAAACCCTTTTAGCCAATCG-3′) and PR2 (5′-GTTTGGGTGGGAGAAGACTGATG-3′); SPR3, PF3 (5′-GCTCCTCCCTCTTTCTTTCTC-3′) and PR3 (5′-CTCTGCGAAAGGAAGAACC-3′); SPR4, PF4 (5′-TACAAGTGGGGGCATATAGG-3′) and PR4 (5′-GTCGCAAATATGATGGACGC-3′); and Actin1, JP1595 (5′-CGTTTCGCTTTCCTTAGTGTTAGCT-3′) and JP1596 (5′-AGCGAACGGATCTAGAGACTCACCTTG-3′).

IP-RT-PCR

IP-RT-PCR with ChIP was performed as described by Wang et al. (2008), except that the sonication step was omitted. Briefly, 14- to 16-d-old seedlings were vacuum infiltrated with 1% formaldehyde for cross-linking and, after the cross-linking was quenched, the seedlings were ground in liquid nitrogen. Myc-specific antibody (Upstate Biotechnology) was added to the solution, which was precleared with salmon sperm DNA/Protein A agarose beads (Upstate Biotechnology). After subsequent incubation with salmon sperm DNA/Protein A agarose beads, immunocomplexes were precipitated and eluted from the beads. The cross-links were reversed, and residual proteins in the immunocomplexes were removed by incubation with proteinase K, followed by phenol/chloroform extraction. The recovered RNA was reverse transcribed as described for RT-PCR using either the *SOC1* 7th-exon-specific primer, SOC1EX7R (5′-CTGCAGCTAGAGCTTTCTC-3′; Figure 6) or an oligo(dT) primer (Figure 7). For *SOC1*, the amount of cDNA reverse transcribed from the immunoprecipitated RNA was determined by PCR amplification of five different regions of the *SOC1* pre-mRNA. The primer pair sequences used for each PCR reaction are as follows: SIT1, SOC1Fa and SOC1EX5R (5′-GCTCCTCGATTGAGCATGTTCC-3′); SIT2, SOC1Fa and SOC1EX3R

(5′-GCTGACTCGATCCTTAGTATGCC-3′); SIT3, SOC1F (5′-TGAGGCATACTAAGGATCGAGTCAG-3′) and SOC1EX5R; SIT4, SOC1F and SOC6INT (5′-GCAAGCACAAGAGGCTTAC-3′); and SIT5, SOC1F and SOC1R (5′-GCGTCTCTACTTCAGAACTTGGGC-3′). For transcripts in Figure 7C, the primers used for RT-PCR analyses were also used to determine the amount of cDNAs generated after IP-RT.

RT-PCR and qPCR Analyses

Reverse transcription was performed with Superscript II (Invitrogen Life Technologies) and an oligo(dT) primer according to the manufacturer's instructions using 2.5 μg of total RNA isolated as described above. PCR was performed using first-strand DNA with i-Taq DNA polymerase (iNtRON Biotechnology) and the following primer pairs for each gene: *CRY2* (5′-GACAATCCCGCGTTACAAGGCG-3′ and 5′-CGTTGTAACGAACAGCCGAAGG-3′), *FT* (5′-GCTACAACTGGAACAACCTTTGGCAAT-3′ and 5′-TATAGGCATCATCACCGTTCGTTACTC-3′), *GI* (5′-GTTGTCCTTCAGGCTGAAAG-3′ and 5′-TGTGGAGAGCAAGCTGTGAG-3′), *CO* (5′-AAACTCTTTCAGCTCCATGACCACTACT-3′ and 5′-CCATGGATGAAATGTATGCGTTATGGTTA-3′), *FLC* (5′-TTCTCCAAACGTCGCAACGGTCTC-3′ and 5′-GATTTGTCCAGCAGGTGACATCTC-3′), *FLM* (5′-GGCATAACCCTTATCGGAGATTTGAAGC-3′ and 5′-ACACAAACTCTGATCTTGTCTCCGAAGG-3′), *MAF2* (5′-GGGTCTCCGGTGATTAGG-3′ and 5′-CTTGAGCAGCGGAAGAGTCTCCC-3′), *MAF3* (5′-CATTTTGGGTCCCCGGTGG-3′ and 5′-GCGAAAGAGTCTCCGGTAC-3′), *MAF4* (5′-CGTTCAGTGTCTCCGGCGAG-3′ and 5′-CGTAGCAGGGGGAAGAAGAGG-3′), *MAF5* (5′-TTCAGGATCTCCGACCAG-3′ and 5′-CAGCCGTTGATGATTGGTGG-3′), *SVP* (5′-CGCTCTCATCATCTTCTCTTCCAC-3′ and 5′-GCTCGTTCTCTTCCGTTAGTTGC-3′), and *UBQ* (5′-GATCTTTGCCGGAAAACAATTGGAGGATGGT-3′ and 5′-CGACTTGTCATTAGAAAGAAAGAGATAACAGG-3′). The primers used for *SOC1* RT-PCR are described above in the IP-RT-PCR section. The RT-PCR primers used for *FCA*, *FY*, *FVE*, and *FLD* were as previously described (Han et al., 2007), and those used to evaluate NMD in *elf9* alleles were described previously (Hori and Watanabe, 2005; Arciga-Reyes et al., 2006). The abundance of the PCR products was quantified based on the images using Metamorph software (Universal Imaging). qPCR was performed in 96-well blocks with an Applied Biosystems 7300 real-time PCR system using the SYBR Green I master mix (Bio-Rad) in a volume of 20 μL. The reactions were performed in triplicate for each run. The comparative $_{\Delta\Delta}$CT method was used to evaluate the relative quantities of each amplified product in the samples. The threshold cycle (Ct) was automatically determined for each reaction by the system set with default parameters. The specificity of the PCR was determined by melt curve analysis of the amplified products using the standard method installed in the system.

Complementation of *elf9-1*

To complement the *elf9-1* mutant, a 6.1-kb genomic fragment of *ELF9* containing 0.6 kb of the 5′ upstream region, the entire coding region, and the 3′ UTR of *ELF9* was generated by PCR amplification using primers ELF9GUS-Pst (5′-aaactgcagACTCTTCTACTGGTGATGAAGAAG-3′) and ELF9-Kpn (5′-cgggtaccTGCGAATAAAACATTCCTCGT-3′). The restriction sites used for cloning are underlined, and sequences corresponding to *ELF9* genomic DNA appear in capital letters. The resulting PCR product was digested with *Pst*1 and *Kpn*I and ligated into pPZP211-G (Noh et al., 2001) between the *Pst*1 and *Kpn*I sites. The *elf9-1* mutant plants were transformed by infiltration (Clough and Bent, 1998) using *Agrobacterium tumefaciens* strain GV3101 containing the construct. Transgenic plants were selected on MS media with 50 μg/mL of kanamycin (Sigma-Aldrich) and evaluated for changes in flowering time.

CHX Treatment

Leaves of 38-d-old wild-type Ws and *elf9-1* plants grown in SDs were harvested at ZT8 and treated with 20 μM CHX (CALBIOCHEM) as described previously (Hori and Watanabe, 2005). Briefly, the leaf sections were vacuum-infiltrated with the CHX solution or with water as a control for 5 min and incubated at room temperature for 4 h. Total RNA was extracted and used for RT-PCR analyses.

GUS and GFP Assays

To construct the *ELF9*$_{pro}$*:ELF9:GUS* translational fusion construct, a 4.7-kb genomic fragment of *ELF9* containing the 0.6-kb 5′ upstream region and the entire coding region was generated by PCR amplification using ELF9GUS-Pst (5′-aaactgcagACTCTTCTACTGGTGATGAAGAAG-3′) and ELF9GUS-Sma (5′-acccgggCTCAGCAGCTTCCAGTTC-3′) as primers. The restriction sites for cloning are underlined in the primer sequences, and sequences corresponding to the *ELF9* genomic DNA are in capital letters. The resulting PCR product was digested with *Pst*I and *Sma*I and ligated into pPZP211-GUS (Noh and Amasino, 2003) digested with the same enzymes. The *CaMV35S*$_{pro}$*:ELF9:GFP* fusion construct was generated by PCR amplification of the 1.6-kb *ELF9* cDNA fragment using ELF9GFP-Sal (5′-gtcgacATGTCAGACTCTGATAATC-3′) and ELF9GFP-Sma (5′-acccgggaaCTCAGCAGCTTCCAGTTC-3′) as primers. After restriction digestion with *Sal*I-*Sma*I, the PCR product was ligated into JJ461 (Han et al., 2007). Wild-type Ws plants were transformed using *A. tumefaciens* strain ABI containing the *ELF9*$_{pro}$*:ELF9:GUS* or the *CaMV35S*$_{pro}$*:ELF9:GFP* construct by infiltration (Clough and Bent, 1998). Histochemical GUS staining was performed as described by Schomburg et al. (2001) using transgenic plants, which were selected as described below. Transgenic plants containing the *ELF9*$_{pro}$*:ELF9:GUS* or the *CaMV35S*$_{pro}$*:ELF9:GFP* construct were selected on MS media with 50 μg/mL of kanamycin (Sigma-Aldrich) or 50 μg/mL of hygromycin (Sigma-Aldrich), respectively. The GFP fusion protein was excited at 488 nm, and the signals were filtered with an HQ515/30 emission filter using a confocal laser scanning microscope (MRC-1024; Bio-Rad).

ELF9 Overexpression

To overexpress *ELF9*, 4.1 kb of genomic DNA containing the entire coding region of *ELF9* was generated by PCR amplification using ELF9OEF-BamH (5′-ggatccCCATGTCAGACTCTGATAATC-3′) and ELF9OER-Sma (5′-acccgggCTCAGCAGCTTCCAGTTC-3′) as primers. The restriction sites used for cloning are underlined, and sequences corresponding to *ELF9* genomic DNA are indicated in capital letters. The resulting PCR product was digested with *Bam*HI-*Sma*I and ligated into myc-pBA (Zhou et al., 2005) digested with *Bam*HI-*Sna*BI. Transformation of wild-type Ws with *A. tumefaciens* strain GV3101 carrying the construct and selection of transgenic lines were performed on MS media containing 50 μg/mL of BASTA (glufosinate ammonium; Aventis). Two representative lines demonstrating robust expression of *ELF9* mRNA were crossed with the *elf9-1* mutants. Homozygous lines were selected in the T3 generation and evaluated for changes in flowering time.

SOC1 Overexpression

To overexpress *SOC1*, a 3.3-kb fragment of genomic DNA containing the 5′ UTR and entire coding region of *SOC1* was generated by PCR using primers SOC1OEF (5′-acccgggGCTCCTCCCTCTTTCTTTCTC-3′) and SOC1OER (5′-cggatccCTTTCTTGAAGAACAAGGTAACC-3′). The restriction sites used for cloning are underlined, and the sequences corresponding to *SOC1* genomic DNA are indicated in capital letters. The resulting PCR product was digested with *Xma*I-*Bam*HI and ligated into myc-pBA (Zhou et al., 2005) digested with the same enzymes. After

transformation with *A. tumefaciens* strain GV3101 carrying the construct, transgenic Ws plants were selected on MS media containing 50 μg/mL of BASTA. Three transgenic lines (SOC1OE1, SOC1OE2, and SOC1OE3) displaying robust expression of *SOC1* were selected.

Accession Numbers

Sequence data from this article can be found in the Arabidopsis Genome Initiative, GenBank/EMBL, or Phytozome (http://www.phytozome.net) databases under the following accession numbers: *ELF9*, *At5g16260*; Pt EFL9a, ID 226768; Pt ELF9b, ID 564123; Os ELF9, AK111787; Sb ELF9a, ID Sbi_0.40096; and Sb ELF9b, ID Sbi_0.7552.

Supplemental Data

The following materials are available in the online version of this article.

Supplemental Figure 1. Spatial Expression Pattern of ELF9 and Its Nuclear Localization.

Supplemental Figure 2. RT-PCR Analysis at Various Amplification Cycles for Primer Pairs Used in the Expression Analysis of This Study.

Supplemental Figure 3. *SOC1* Splicing Variants Detected in *sso14* via RT-PCR Analyses.

Supplemental Figure 4. *ELF9* Overexpression.

Supplemental Figure 5. Schematic Diagram of the *SOC1* 5′ UTR and the Coding Region Showing Multiple Initiator Codons.

Supplemental Figure 6. *CaMV35S* Promoter-Driven Overexpression of *SOC1* in Wild-Type Ws Plants.

Supplemental Figure 7. Sequence Comparison between the RRMs of ELF9 and Its Homologs in Other Plant Species.

ACKNOWLEDGMENTS

We thank Narry Kim for an insightful discussion, Brendan Davies and Samantha Broad for sharing *upf1* and *upf3* mutants, and Ilha Lee for providing *sso14*. This work was supported by the Global Research Laboratory Program of the Ministry of Education, Science, and Technology/Korea Foundation for International Cooperation of Science and Technology, by the Plant Diversity Research Center, and by the BioGreen21 Program of the Rural Development Administration. B.N. was supported by a grant from the Ministry of Education, Science, and Technology/Korea Science and Engineering Foundation to the Environmental Biotechnology National Core Research Center (R15-2003-012-01001-0) and by grants from the Korea Research Foundation (KRF-2007-313-C00703 and KRF-2006-312-C00672). H.-R.S. and J.-N.C. were supported by the BK21 Program. Work in R.M.A.'s lab was also supported by National Institutes of Health Grant 1R01GM079525 and National Science Foundation Grant 0209786.

Received December 2, 2008; revised March 27, 2009; accepted April 5, 2009; published April 17, 2009.

REFERENCES

Abe, M., Kobayashi, Y., Yamamoto, S., Daimon, Y., Yamaguchi, A., Ikeda, Y., Ichinoki, H., Notaguchi, M., Goto, K., and Araki, T. (2005). FD, a bZIP protein mediating signals from the floral pathway integrator FT at the shoot apex. Science **309:** 1052–1056.

Arciga-Reyes, L., Wootton, L., Kieffer, M., and Davies, B. (2006). UPF1 is required for nonsense-mediated mRNA decay (NMD) and RNAi in Arabidopsis. Plant J. **47:** 480–489.

Ausin, I., Alonso-Blanco, C., Jarillo, J.A., Ruiz-Garcia, L., and Martinez-Zapater, J.M. (2004). Regulation of flowering time by FVE, a retinoblastoma-associated protein. Nat. Genet. **36:** 162–166.

Bäurle, I., and Dean, C. (2006). The timing of developmental transitions in plants. Cell **125:** 655–664.

Bezerra, I.C., Michaels, S.D., Schomburg, F.M., and Amasino, R.M. (2004). Lesions in the mRNA cap-binding gene ABA HYPERSENSITIVE 1 suppress FRIGIDA-mediated delayed flowering in Arabidopsis. Plant J. **40:** 112–119.

Blázquez, M.A., and Weigel, D. (2000). Integration of floral inductive signals in Arabidopsis. Nature **404:** 889–892.

Carter, M.S., Doskow, J., Morris, P., Li, S., Nhim, R.P., Sandstedt, S., and Wilkinson, M.F. (1995). A regulatory mechanism that detects premature nonsense codons in T-cell receptor transcripts in vivo is reversed by protein synthesis inhibitors in vitro. J. Biol. Chem. **270:** 28995–29003.

Chen, X., and Meyerowitz, E.M. (1999). HUA1 and HUA2 are two members of the floral homeotic AGAMOUS pathway. Mol. Cell **3:** 349–360.

Cheng, Y., Kato, N., Wang, W., Li, J., and Chen, X. (2003). Two RNA binding proteins, HEN4 and HUA1, act in the processing of AGAMOUS pre-mRNA in *Arabidopsis thaliana*. Dev. Cell **4:** 53–66.

Clough, S.J., and Bent, A.F. (1998). Floral dip: A simplified method for Agrobacterium-mediated transformation of *Arabidopsis thaliana.* Plant J. **16:** 735–743.

Dahlseid, J.N., Lew-Smith, J., Lelivelt, M.J., Enomoto, S., Ford, A., Desruisseaux, M., McClellan, M., Lue, N., Culbertson, M.R., and Berman, J. (2003). mRNAs encoding telomerase components and regulators are controlled by UPF genes in *Saccharomyces cerevisiae*. Eukaryot. Cell **2:** 134–142.

Deal, R.B., Kandasamy, M.K., McKinney, E.C., and Meagher, R.B. (2005). The nuclear actin-related protein ARP6 is a pleiotropic developmental regulator required for the maintenance of FLOWERING LOCUS C expression and repression of flowering in *Arabidopsis*. Plant Cell **17:** 2633–2646.

Doyle, M.R., Bizzell, C.M., Keller, M.R., Michaels, S.D., Song, J., Noh, Y.S., and Amasino, R.M. (2005). HUA2 is required for the expression of floral repressors in *Arabidopsis thaliana*. Plant J. **41:** 376–385.

El-Din El-Assal, S., Alonso-Blanco, C., Peeters, A.J., Wagemaker, C., Weller, J.L., and Koornneef, M. (2003). The role of cryptochrome 2 in flowering in Arabidopsis. Plant Physiol. **133:** 1504–1516.

Han, S.K., Song, J.D., Noh, Y.S., and Noh, B. (2007). Role of plant CBP/p300-like genes in the regulation of flowering time. Plant J. **49:** 103–114.

He, Y., and Amasino, R.M. (2005). Role of chromatin modification in flowering-time control. Trends Plant Sci. **10:** 30–35.

He, Y., Doyle, M.R., and Amasino, R.M. (2004). PAF1-complex-mediated histone methylation of FLOWERING LOCUS C chromatin is required for the vernalization-responsive, winter-annual habit in Arabidopsis. Genes Dev. **18:** 2774–2784.

He, Y., Michaels, S.D., and Amasino, R.M. (2003). Regulation of flowering time by histone acetylation in Arabidopsis. Science **302:** 1751–1754.

Hepworth, S.R., Valverde, F., Ravenscroft, D., Mouradov, A., and Coupland, G. (2002). Antagonistic regulation of flowering-time gene SOC1 by CONSTANS and FLC via separate promoter motifs. EMBO J. **21:** 4327–4337.

Hori, K., and Watanabe, Y. (2005). UPF3 suppresses aberrant spliced mRNA in Arabidopsis. Plant J. **43:** 530–540.

Hugouvieux, V., Kwak, J.M., and Schroeder, J.I. (2001). An mRNA cap binding protein, ABH1, modulates early abscisic acid signal transduction in Arabidopsis. Cell **106:** 477–487.

Imaizumi, T., Schultz, T.F., Harmon, F.G., Ho, L.A., and Kay, S.A. (2005). FKF1 F-box protein mediates cyclic degradation of a repressor of CONSTANS in Arabidopsis. Science **309:** 293–297.

Isken, O., and Maquat, L.E. (2008). The multiple lives of NMD factors: Balancing roles in gene and genome regulation. Nat. Rev. Genet. **9:** 699–712.

Jang, S., Marchal, V., Panigrahi, K.C., Wenkel, S., Soppe, W., Deng, X.W., Valverde, F., and Coupland, G. (2008). Arabidopsis COP1 shapes the temporal pattern of CO accumulation conferring a photoperiodic flowering response. EMBO J. **27:** 1277–1288.

Kim, S., Koh, J., Yoo, M.J., Kong, H., Hu, Y., Ma, H., Soltis, P.S., and Soltis, D.E. (2005). Expression of floral MADS-box genes in basal angiosperms: Implications for the evolution of floral regulators. Plant J. **43:** 724–744.

Koornneef, M., Blankestijn-de Vries, H., Hanhart, C., Soppe, W., and Peeters, T. (1994). The phenotype of some late-flowering mutants is enhanced by a locus on chromosome 5 that is not effective in the Landsberg *erecta* wild-type. Plant J. **6:** 911–919.

Koornneef, M., Hanhart, C.J., and van der Veen, J.H. (1991). A genetic and physiological analysis of late flowering mutants in *Arabidopsis thaliana*. Mol. Gen. Genet. **229:** 57–66.

Kuhn, J.M., Breton, G., and Schroeder, J.I. (2007). mRNA metabolism of flowering-time regulators in wild-type Arabidopsis revealed by a nuclear cap binding protein mutant, abh1. Plant J. **50:** 1049–1062.

Laubinger, S., Marchal, V., Le Gourrierec, J., Wenkel, S., Adrian, J., Jang, S., Kulajta, C., Braun, H., Coupland, G., and Hoecker, U. (2006). Arabidopsis SPA proteins regulate photoperiodic flowering and interact with the floral inducer CONSTANS to regulate its stability. Development **133:** 3213–3222.

Lee, H., Suh, S.S., Park, E., Cho, E., Ahn, J.H., Kim, S.G., Lee, J.S., Kwon, Y.M., and Lee, I. (2000). The AGAMOUS-LIKE 20 MADS domain protein integrates floral inductive pathways in Arabidopsis. Genes Dev. **14:** 2366–2376.

Lee, I., Michaels, S.D., Masshardt, A.S., and Amasino, R.M. (1994). The late-flowering phenotype of *FRIGIDA* and mutations in *LUMINIDEPENDENS* is suppressed in the Landsberg *erecta* strain of *Arabidopsis.* Plant J. **6:** 903–909.

Lee, J., Oh, M., Park, H., and Lee, I. (2008). SOC1 translocated to the nucleus by interaction with AGL24 directly regulates leafy. Plant J. **55:** 832–843.

Lee, T.I., et al. (2006). Control of developmental regulators by Polycomb in human embryonic stem cells. Cell **125:** 301–313.

Lelivelt, M.J., and Culbertson, M.R. (1999). Yeast Upf proteins required for RNA surveillance affect global expression of the yeast transcriptome. Mol. Cell. Biol. **19:** 6710–6719.

Li, D., Liu, C., Shen, L., Wu, Y., Chen, H., Robertson, M., Helliwell, C.A., Ito, T., Meyerowitz, E., and Yu, H. (2008). A repressor complex governs the integration of flowering signals in Arabidopsis. Dev. Cell **15:** 110–120.

Lim, M.H., Kim, J., Kim, Y.S., Chung, K.S., Seo, Y.H., Lee, I., Hong, C.B., Kim, H.J., and Park, C.M. (2004). A new *Arabidopsis* gene, FLK, encodes an RNA binding protein with K homology motifs and regulates flowering time via FLOWERING LOCUS C. Plant Cell **16:** 731–740.

Liu, C., Chen, H., Er, H.L., Soo, H.M., Kumar, P.P., Han, J.H., Liou, Y.C., and Yu, H. (2008a). Direct interaction of AGL24 and SOC1 integrates flowering signals in Arabidopsis. Development **135:** 1481–1491.

Liu, L.J., Zhang, Y.C., Li, Q.H., Sang, Y., Mao, J., Lian, H.L., Wang, L., and Yang, H.Q. (2008b). COP1-mediated ubiquitination of CONSTANS is implicated in cryptochrome regulation of flowering in Arabidopsis. Plant Cell **20:** 292–306.

Liu, S., Yu, Y., Ruan, Y., Meyer, D., Wolff, M., Xu, L., Wang, N., Steinmetz, A., and Shen, W.H. (2007). Plant SET- and RING-associated domain proteins in heterochromatinization. Plant J. **52:** 914–926.

Liu, Y.G., Mitsukawa, N., Oosumi, T., and Whittier, R.F. (1995). Efficient isolation and mapping of *Arabidopsis thaliana* T-DNA insert junctions by thermal asymmetric interlaced PCR. Plant J. **8:** 457–463.

Lorkovic, Z.J., and Barta, A. (2002). Genome analysis: RNA recognition motif (RRM) and K homology (KH) domain RNA-binding proteins from the flowering plant *Arabidopsis thaliana*. Nucleic Acids Res. **30:** 623–635.

Macknight, R., Bancroft, I., Page, T., Lister, C., Schmidt, R., Love, K., Westphal, L., Murphy, G., Sherson, S., Cobbett, C., and Dean, C. (1997). FCA, a gene controlling flowering time in Arabidopsis, encodes a protein containing RNA-binding domains. Cell **89:** 737–745.

Macknight, R., Duroux, M., Laurie, R., Dijkwel, P., Simpson, G., and Dean, C. (2002). Functional significance of the alternative transcript processing of the Arabidopsis floral promoter FCA. Plant Cell **14:** 877–888.

Michaels, S.D., and Amasino, R.M. (1999). The gibberellic acid biosynthesis mutant ga1-3 of Arabidopsis thaliana is responsive to vernalization. Dev. Genet. **25:** 194–198.

Mizoguchi, T., Wright, L., Fujiwara, S., Cremer, F., Lee, K., Onouchi, H., Mouradov, A., Fowler, S., Kamada, H., Putterill, J., and Coupland, G. (2005). Distinct roles of GIGANTEA in promoting flowering and regulating circadian rhythms in *Arabidopsis*. Plant Cell **17:** 2255–2270.

Moon, J., Suh, S.S., Lee, H., Choi, K.R., Hong, C.B., Paek, N.C., Kim, S.G., and Lee, I. (2003). The SOC1 MADS-box gene integrates vernalization and gibberellin signals for flowering in Arabidopsis. Plant J. **35:** 613–623.

Murashige, T., and Skoog, F. (1962). A revised medium for rapid growth and bioassays with tobacco tissue culture. Physiol. Plant. **15:** 473–477.

Ni, J.Z., Grate, L., Donohue, J.P., Preston, C., Nobida, N., O'Brien, G., Shiue, L., Clark, T.A., Blume, J.E., and Ares, M., Jr. (2007). Ultraconserved elements are associated with homeostatic control of splicing regulators by alternative splicing and nonsense-mediated decay. Genes Dev. **21:** 708–718.

Noh, B., Lee, S.H., Kim, H.J., Yi, G., Shin, E.A., Lee, M., Jung, K.J., Doyle, M.R., Amasino, R.M., and Noh, Y.S. (2004). Divergent roles of a pair of homologous jumonji/zinc-finger-class transcription factor proteins in the regulation of *Arabidopsis* flowering time. Plant Cell **16:** 2601–2613.

Noh, B., Murphy, A.S., and Spalding, E.P. (2001). Multidrug resistance-like genes of *Arabidopsis* required for auxin transport and auxin-mediated development. Plant Cell **13:** 2441–2454.

Noh, B., and Noh, Y.-S. (2006). Chromatin-mediated regulation of flowering time in Arabidopsis. Physiol. Plant. **126:** 484–493.

Noh, Y.S., and Amasino, R.M. (2003). *PIE1*, an ISWI family gene, is required for *FLC* activation and floral repression in Arabidopsis. Plant Cell **15:** 1671–1682.

Parenicova, L., de Folter, S., Kieffer, M., Horner, D.S., Favalli, C., Busscher, J., Cook, H.E., Ingram, R.M., Kater, M.M., Davies, B., Angenent, G.C., and Colombo, L. (2003). Molecular and phylogenetic analyses of the complete MADS box transcription factor family in *Arabidopsis*: New openings to the MADS world. Plant Cell **15:** 1538–1551.

Putterill, J., Robson, F., Lee, K., Simon, R., and Coupland, G. (1995). The CONSTANS gene of Arabidopsis promotes flowering and encodes

a protein showing similarities to zinc finger transcription factors. Cell **80:** 847–857.

Quesada, V., Macknight, R., Dean, C., and Simpson, G.G. (2003). Autoregulation of FCA pre-mRNA processing controls Arabidopsis flowering time. EMBO J. **22:** 3142–3152.

Ratcliffe, O.J., Kumimoto, R.W., Wong, B.J., and Riechmann, J.L. (2003). Analysis of the Arabidopsis MADS AFFECTING FLOWERING gene family: MAF2 prevents vernalization by short periods of cold. Plant Cell **15:** 1159–1169.

Ruiz-Echevarria, M.J., and Peltz, S.W. (2000). The RNA binding protein Pub1 modulates the stability of transcripts containing upstream open reading frames. Cell **101:** 741–751.

Schomburg, F.M., Bizzell, C.M., Lee, D.J., Zeevaart, J.A., and Amasino, R.M. (2003). Overexpression of a novel class of gibberellin 2-oxidases decreases gibberellin levels and creates dwarf plants. Plant Cell **15:** 151–163.

Schomburg, F.M., Patton, D.A., Meinke, D.W., and Amasino, R.M. (2001). FPA, a gene involved in floral induction in *Arabidopsis*, encodes a protein containing RNA-recognition motifs. Plant Cell **13:** 1427–1436.

Scortecci, K.C., Michaels, S.D., and Amasino, R.M. (2001). Identification of a MADS-box gene, FLOWERING LOCUS M, that represses flowering. Plant J. **26:** 229–236.

Searle, I., and Coupland, G. (2004). Induction of flowering by seasonal changes in photoperiod. EMBO J. **23:** 1217–1222.

Searle, I., He, Y., Turck, F., Vincent, C., Fornara, F., Krober, S., Amasino, R.A., and Coupland, G. (2006). The transcription factor FLC confers a flowering response to vernalization by repressing meristem competence and systemic signaling in Arabidopsis. Genes Dev. **20:** 898–912.

Sheldon, C.C., Burn, J.E., Perez, P.P., Metzger, J., Edwards, J.A., Peacock, W.J., and Dennis, E.S. (1999). The FLF MADS box gene: A repressor of flowering in *Arabidopsis* regulated by vernalization and methylation. Plant Cell **11:** 445–458.

Shyu, A.B., Wilkinson, M.F., and van Hoof, A. (2008). Messenger RNA regulation: To translate or to degrade. EMBO J. **27:** 471–481.

Simpson, G.G., and Dean, C. (2002). Arabidopsis, the Rosetta stone of flowering time? Science **296:** 285–289.

Simpson, G.G., Dijkwel, P.P., Quesada, V., Henderson, I., and Dean, C. (2003). FY is an RNA 3′ end-processing factor that interacts with FCA to control the Arabidopsis floral transition. Cell **113:** 777–787.

Squazzo, S.L., O'Geen, H., Komashko, V.M., Krig, S.R., Jin, V.X., Jang, S.W., Margueron, R., Reinberg, D., Green, R., and Farnham, P.J. (2006). Suz12 binds to silenced regions of the genome in a cell-type-specific manner. Genome Res. **16:** 890–900.

Stock, J.K., Giadrossi, S., Casanova, M., Brookes, E., Vidal, M., Koseki, H., Brockdorff, N., Fisher, A.G., and Pombo, A. (2007). Ring1-mediated ubiquitination of H2A restrains poised RNA polymerase II at bivalent genes in mouse ES cells. Nat. Cell Biol. **9:** 1428–1435.

Sung, S., and Amasino, R.M. (2005). Remembering winter: Toward a molecular understanding of vernalization. Annu. Rev. Plant Biol. **56:** 491–508.

Thompson, J.D., Higgins, D.G., and Gibson, T.J. (1994). CLUSTAL W: Improving the sensitivity of progressive multiple sequence alignment through sequence weighting, position-specific gap penalties and weight matrix choice. Nucleic Acids Res. **22:** 4673–4680.

Wang, X., Arai, S., Song, X., Reichart, D., Du, K., Pascual, G., Tempst, P., Rosenfeld, M.G., Glass, C.K., and Kurokawa, R. (2008). Induced ncRNAs allosterically modify RNA-binding proteins in cis to inhibit transcription. Nature **454:** 126–130.

Welch, E.M., and Jacobson, A. (1999). An internal open reading frame triggers nonsense-mediated decay of the yeast SPT10 mRNA. EMBO J. **18:** 6134–6145.

Wigge, P.A., Kim, M.C., Jaeger, K.E., Busch, W., Schmid, M., Lohmann, J.U., and Weigel, D. (2005). Integration of spatial and temporal information during floral induction in Arabidopsis. Science **309:** 1056–1059.

Yan, D., Perriman, R., Igel, H., Howe, K.J., Neville, M., and Ares, M., Jr. (1998). CUS2, a yeast homolog of human Tat-SF1, rescues function of misfolded U2 through an unusual RNA recognition motif. Mol. Cell. Biol. **18:** 5000–5009.

Zeevaart, J.A.D. (2008). Leaf-produced floral signals. Curr. Opin. Plant Biol. **11:** 541–547.

Zhou, Q., Hare, P.D., Yang, S.W., Zeidler, M., Huang, L.F., and Chua, N.H. (2005). FHL is required for full phytochrome A signaling and shares overlapping functions with FHY1. Plant J. **43:** 356–370.

Zhou, Q., and Sharp, P.A. (1996). Tat-SF1: Cofactor for stimulation of transcriptional elongation by HIV-1 Tat. Science **274:** 605–610.